iScience

CellPress

Article

Regenerative Adaptation to Electrochemical Perturbation in Planaria: A Molecular Analysis of Physiological Plasticity

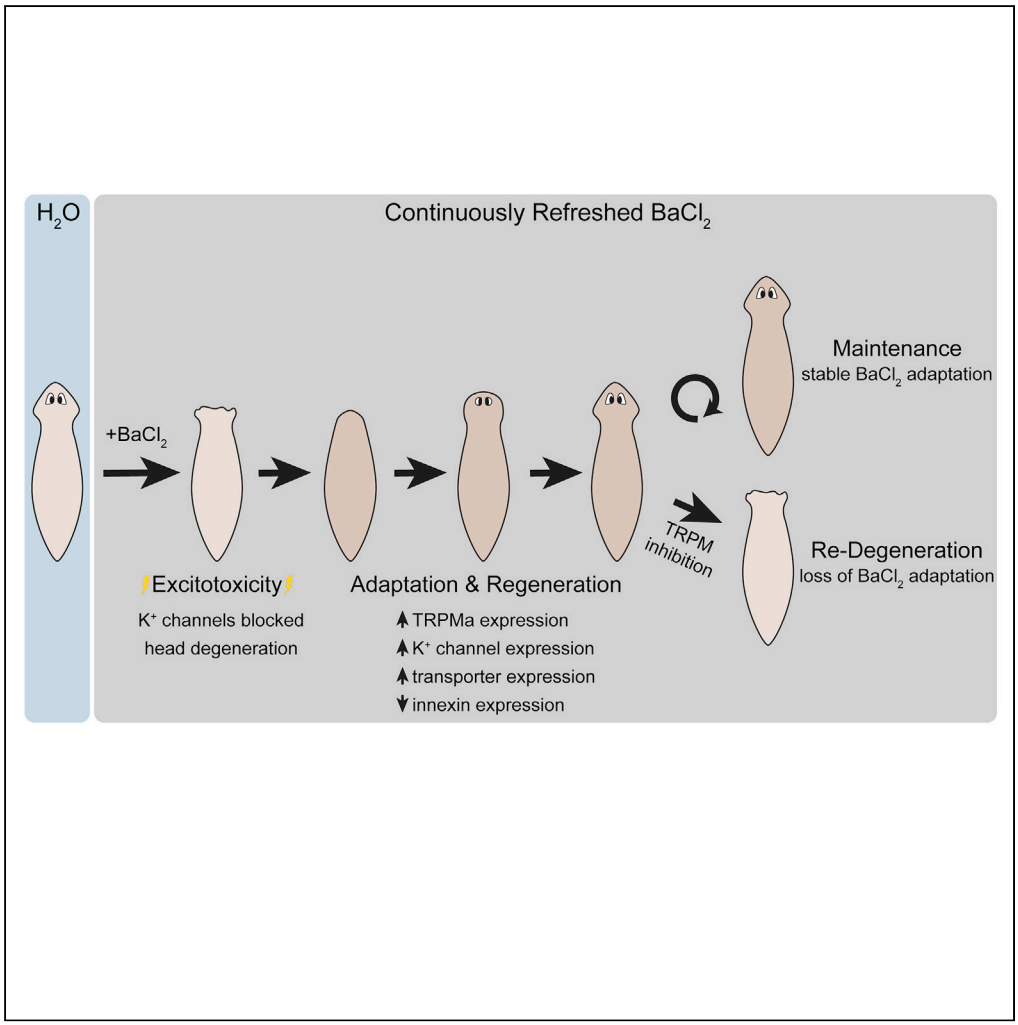

Maya Emmons-Bell, Fallon Durant, Angela Tung, ..., Devon Davidian, Junji Morokuma, Michael Levin

michael.levin@tufts.edu

HIGHLIGHTS

Exposure to $BaCl_2$ causes the heads of *Dugesia japonica* to degenerate

Prolonged exposure to $BaCl_2$ results in regeneration of a $BaCl_2$-insensitive head

Ion channel expression is altered in the head to compensate for excitotoxic stress

TRPMa is upregulated in $BaCl_2$-treated animals; blocking TRPM prevents adaptation

Emmons-Bell et al., iScience *22*, 147–165
December 20, 2019
https://doi.org/10.1016/j.isci.2019.11.014

iScience

CellPress

Article

Regenerative Adaptation to Electrochemical Perturbation in Planaria: A Molecular Analysis of Physiological Plasticity

Maya Emmons-Bell,[1,2,4,6] Fallon Durant,[1,2,5,6] Angela Tung,[1,2] Alexis Pietak,[1] Kelsie Miller,[1] Anna Kane,[1] Christopher J. Martyniuk,[3] Devon Davidian,[1,2] Junji Morokuma,[1,2] and Michael Levin[1,2,7,*]

SUMMARY

Anatomical homeostasis results from dynamic interactions between gene expression, physiology, and the external environment. Owing to its complexity, this cellular and organism-level phenotypic plasticity is still poorly understood. We establish planarian regeneration as a model for acquired tolerance to environments that alter endogenous physiology. Exposure to barium chloride ($BaCl_2$) results in a rapid degeneration of anterior tissue in *Dugesia japonica*. Remarkably, continued exposure to fresh solution of $BaCl_2$ results in regeneration of heads that are insensitive to $BaCl_2$. RNA-seq revealed transcriptional changes in $BaCl_2$-adapted heads that suggests a model of adaptation to excitotoxicity. Loss-of-function experiments confirmed several predictions: blockage of chloride and calcium channels allowed heads to survive initial $BaCl_2$ exposure, inducing adaptation without prior exposure, whereas blockade of TRPM channels reversed adaptation. Such highly adaptive plasticity may represent an attractive target for biomedical strategies in a wide range of applications beyond its immediate relevance to excitotoxicity preconditioning.

INTRODUCTION

A fundamental challenge faced by all living things is survival in an uncertain and changing environment. One of the fundamental goals of biology and medicine is to understand how physiology and morphology, whether at the cell or organism level, adjusts to stress—conditions that are not conducive to continued health and reproduction. Living tissues are confronted with continuous environmental challenge at all scales of size and organization, from exposure to agents that damage DNA and produce reactive oxygen species at the level of single cells to secreted factors and cell group activity that drive embryogenesis and repair/regeneration; to the physiological functions of immune, circulatory, and endocrine systems; and ultimately to the behavior of the entire animal. Thus, all components of an organism must continuously select from a very large space of possible transcriptional, protein-level, and physiological-level responses to adaptively maintain homeostasis along numerous parameters during its lifespan. Understanding this ubiquitous process is vital, with direct applications to reprotoxicology (the ability of embryos to regulate, or fail to regulate, their normal developmental sequence under diverse, potentially teratogenic influences), immunology, aging, and cancer. Harnessing this process is also a goal of regenerative medicine.

Major gaps remain in our understanding of the fundamental biology of computation in living media: how do cellular networks process real-time information toward near-optimal responses? On a population scale, recent work with bacterial persisters and yeast subjected to antibiotic and metabolic stress, respectively, reveals evolutionary aspects of epigenetic tolerance to stressors (Lopez Garcia de Lomana et al., 2017; Samani and Bell, 2016; Gonzalez and Bell, 2013; Kussell et al., 2005; Balaban et al., 2004; Tkachenko, 2018; Lambert and Kussell, 2014). However, experiments in *Drosophila* and other model systems reveal that, even within the lifetime of single individuals (i.e., not via selection), cells have the remarkable ability to execute appropriate responses to stressors (Soen et al., 2015; Elgart et al., 2015; Stern et al., 2012; Soen and Braun, 2000; Karin et al., 2016). This emerging body of work on cellular adaptation and plasticity (Stetina et al., 2015; Prymaczok et al., 2016) is complemented by similar robustness observed at the organ or even whole-organism scale (Pezzulo and Levin, 2015; Brunke and Hube, 2014; Sorek et al., 2013; Freddolino and Tavazoie, 2012).

One of the best examples of large-scale dynamic plasticity is regulative development, which is often able to adjust to drastic injury (Cooke, 1981; Tarkowski, 1961). One example can be seen in the processes that

[1]Allen Discovery Center at Tufts University, Medford, MA 02155, USA

[2]Department of Biology, Tufts University, Medford, MA 02155, USA

[3]Department of Physiological Sciences and Center for Environmental and Human Toxicology, University of Florida Genetics Institute, Interdisciplinary Program in Biomedical Sciences Neuroscience, College of Veterinary Medicine, University of Florida, Gainesville, FL 32611, USA

[4]Present address: University of California, Berkeley, Berkeley, CA 94720, USA

[5]Present address: Harvard University, Cambridge, MA 02138, USA

[6]These authors contributed equally

[7]Lead Contact

*Correspondence: michael.levin@tufts.edu

https://doi.org/10.1016/j.isci.2019.11.014

convert a tadpole face to that of a frog, which requires significant movements of the eyes and other organs to rearrange internal head structures into the correct species-specific outcome. It was recently shown that this is not a hardwired process in which the different components move in pre-determined paths (Vandenberg et al., 2012) and rely on a constant starting state to implement normal frog development. Tadpoles engineered to have scrambled anatomies (eyes, nostrils, and other structures in highly abnormal positions) still usually develop into normal frogs. Thus, the genome encodes a system with the ability to reach the required anatomical state from a range of diverse starting conditions, dynamically adapting to (evolutionarily) unexpected circumstances and readjusting the various tissues as needed to optimize subsequent survival.

Beyond development, metazoan survival throughout the lifespan requires a constant and active resistance to aging, wear and tear, and carcinogenic transformation (Rubin, 1985, 2006, 2007). Moreover, some species are capable of large-scale remodeling and pattern homeostasis throughout their lifespan. Planarians are a class of free-living flatworms that contains many highly regenerative members (Cebrià et al., 2018; Saló et al., 2009). The freshwater planarian *Dugesia japonica* is one such species, able to restore an entire body (including the brain) from a mere fragment, scaling the growth with exquisite precision and ceasing further growth and remodeling when an allometrically correct body plan is complete (Levin et al., 2019; Sahu et al., 2017; Saló et al., 2009). Planarians possess bilateral symmetry, stem cell populations (Hill and Petersen, 2015; Tanaka and Reddien, 2011), and a true centralized brain with numerous complex behavioral responses including learning (Sarnat and Netsky, 1985; Corning and Freed, 1968). They appear to have even conquered the ultimate stressor—aging (Sahu et al., 2017; Petralia et al., 2014). Much progress has been made on the biochemical (Reddien, 2018; Owlarn and Bartscherer, 2016) and physiological/bioelectrical (Lange and Steele, 1978; Chan et al., 2014; Durant et al., 2017; Sullivan et al., 2016; Beane et al., 2011, 2013) control of patterning during regeneration, making them an ideal model system in which one can investigate adaptive responses to novel stimuli that threaten homeostasis.

To establish a model for the study of adaptation at multiple levels of organization, we chose regeneration in *D. japonica* as a context to determine how cellular and body-wide plasticity must cooperate. Owing to the known dependence of planarian remodeling response on bioelectric events (Levin et al., 2019; Durant et al., 2017; Emmons-Bell et al., 2015; Beane et al., 2011, 2013; Oviedo et al., 2010), we challenged planaria with a novel stressor: the non-specific potassium channel blocker barium chloride ($BaCl_2$). The inability to pass potassium ions led to a severe head degeneration. Remarkably, however, the planaria soon regenerated a $BaCl_2$-tolerant head. We analyzed these $BaCl_2$-adapted heads using molecular and physiologic approaches, which revealed an example of transcriptional and physiological plasticity with significant implications for basic biology and neural injury repair.

RESULTS

When Exposed to $BaCl_2$, Planaria Heads Rapidly Degenerate and Subsequently Regenerate with Newly Acquired $BaCl_2$ Resistance

Given the ubiquitous importance of potassium channels in cell physiology, we first asked what would happen to planaria continuously exposed to broad K^+ flux inhibitors. We cultured *D. japonica* flatworms in 1 mM barium chloride ($BaCl_2$), a powerful, widely used, universal potassium channel blocker (Jiang and Mackinnon, 2000; Latorre et al., 1997), which can also affect other divalent cation channels and has been extensively used in invertebrates (Armstrong and Taylor, 1980; Eaton and Brodwick, 1980; Hanrahan et al., 1986). We observed rapid and complete degeneration of the entire head within 72 h (83% of observed worms showed degeneration, SD = 12% across all $BaCl_2$ treatments, Figure 1Ab), consistent with the importance of potassium currents in maintenance and physiology of this complex organ. Remarkably, however, when left to regenerate in fresh $BaCl_2$ solution, the worms regenerated normal heads that were insensitive to the toxic environmental conditions (Figures 1Ac and 1Ad). Although $BaCl_2$ could potentially form insoluble ions with sulfate and carbonate ions present in the Poland Spring water, we ruled out adaptation via reduction of $BaCl_2$ concentration in the media by making sure that media was frequently refreshed. Furthermore, degeneration of anterior tissues was never observed in control culture conditions (Figure 1Aa). Heads regenerated in $BaCl_2$ retained normal size and morphology (Figure 1Ad), and the $BaCl_2$-adapted worms exhibited motion that was not visually different from that of wild-type (WT) worms.

Degeneration involved tissue progressively bubbling off from the very anterior tip of the worm to the plane of the photoreceptors (roughly 1 mm of tissue), with apparent muscular contraction around the

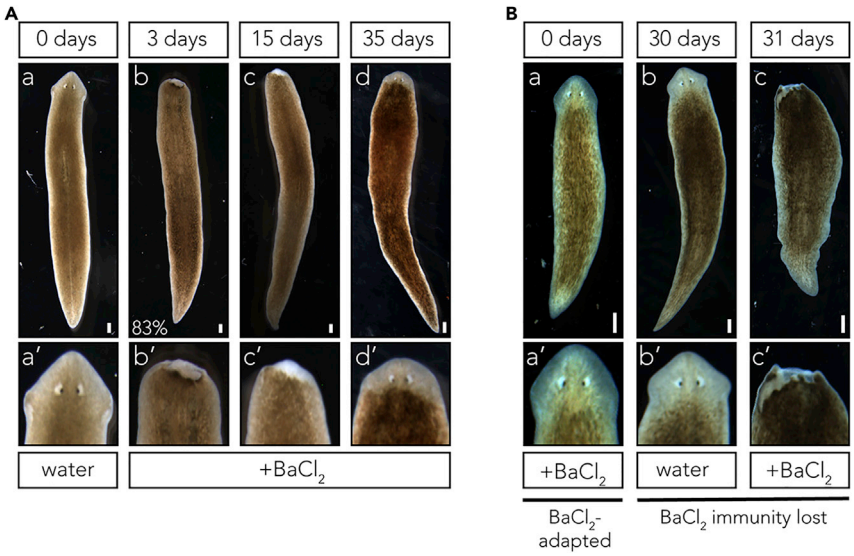

Figure 1. Long-term Exposure to $BaCl_2$ Results in Degeneration of Anterior Tissues and Subsequent Regeneration of Structures That Are Resistant to $BaCl_2$

(A) Whole *D. japonica* worms after treatment in 1 mM $BaCl_2$. (a) Normal worms before treatment. (b) Within 72 h of exposure to $BaCl_2$, the anterior tissues of the planarian degrade and the head deprogresses. This occurs in 83% of worms, SD = 12%. Degeneration occurs through a contraction of tissue at the base of the wound, minimizing tissue loss. (c) After 15 days in $BaCl_2$, *D. japonica* form a blastema and begin to regrow a head. (d) By 37 days of treatment, a new, $BaCl_2$-insensitive head has formed and the worm is phenotypically normal. (a′–d′) 200x zoomed in images of the anterior portion of the worms shown in (a)–(d). Scale bar 0.5 mm. Results representative of three independent biological replicates, N > 50 for each replicate.

(B) (a) *D. japonica* worm after 35 days of $BaCl_2$ treatment. This worm has degenerated and regenerated a head and is now insensitive to $BaCl_2$. (b) *D. japonica* worms are then placed in water for 30 days with no obvious morphological effect. (c) However, upon 24 h of a second $BaCl_2$ treatment, the head degenerates. (a′–c′) 200x zoomed in images of the anterior portion of the worms shown in (a)–(c). Scale bar 0.5 mm. Results representative of three independent biological replicates, N > 50 for each replicate.

degeneration site that minimized internal tissue loss (Figure 1Ab). The process was complete after 72 h in $BaCl_2$ solution. Blastema formation was then initiated, and regenerative processes proceeded, although full regeneration took longer than normal (~4 weeks, as opposed to ~2 weeks, Figure 1Ac). After regeneration of the head, the worms were transferred into a fresh $BaCl_2$ solution and showed no signs of degeneration. We conclude that $BaCl_2$ exposure is acutely toxic to planarian anterior tissues but that the worms have the ability to produce new heads that are completely adapted to this novel, harsh condition.

Acquired Resistance to $BaCl_2$ Is Lost after 30 Days in Water

We then investigated whether the acquired adaptation to $BaCl_2$ was permanent or temporary. *D. japonica* worms were allowed to degenerate and regenerate heads in 1 mM $BaCl_2$ over the course of approximately 35 days (Figure 1Ba). They were then transferred to Poland Spring water for 30 days, with the water refreshed every 7 days (Figure 1Bb). They were then subjected to a second round of 1 mM $BaCl_2$ treatment. All worms displayed characteristic degeneration of anterior tissues after the second round of $BaCl_2$ treatment, revealing that the insensitivity to $BaCl_2$ is lost after 30 days in plain water (Figure 1Bc).

Transcriptionally Profiling the $BaCl_2$-Adapted Head

What is different about the new, $BaCl_2$-compatible heads when compared with the WT planarian head—what changes allow survival in $BaCl_2$ after the initial adaptation? We hypothesized that the conferred resistance to $BaCl_2$ treatment could be due to altered expression of ion channels or pumps that could compensate for, and buffer, the physiological perturbation. To test this hypothesis, we performed RNA sequencing (RNA-seq) and sub-network enrichment analysis (SNEA) on head samples from worms that were either treated with $BaCl_2$ and allowed to regenerate insensitive heads or kept in water following the $BaCl_2$ treatment. Table S1 provides all upregulated and downregulated transcripts identified. We report the total

number of reads generated for each sample as well as a table of the alignment percentage of the reads mapped to the reference in Tables S2 and S3, respectively. GO and SNEA data are provided in Tables S4 and S5, respectively. A subnetwork enrichment was also conducted to enhance the overall dataset and to provide additional information on processes affected in the $BaCl_2$-resistant heads (Table 1).

We detected a number of transcripts that were up- and downregulated after $BaCl_2$ exposure (Table S1, q-value<0.05, change > $\log_2 = 3$), and genes that were only identified in one condition but not the other were listed as highly changed in the appropriate table. Significantly upregulated genes included *metalloendopeptidase, palmitoyl transferase, Slc17a1, NPYR-14, neuroglian, aquaporin, Rab-protein 8, SMAD6/7,* and *Slc2a1* (Table 3). Downregulated genes included *Propionyl-CoA synthetase, CyclinA-like protein, fibronectin, Mariner Mos1 transposase, L-lactate dehydrogenase, TBC1 domain family member 9B, SPSB1, Slc38a2, C3H-zinc finger-containing protein 1, ybox protein 4-like protein, plastin 1,* and *innexin* (Table 4). Interestingly, some ion channels and pumps were differentially expressed (Tables S1, 3, and 4) ($p < 0.05$). For example, *Transient receptor potential ion channel Ma Dj-TRPMa* (Fragment) was upregulated, appearing in the $BaCl_2$-adapted heads but below detection in the wild-type, as well as an uncharacterized voltage-gated potassium channel, *Slc17a-1*, and *NPYR14*.

More broadly, downregulated functional sets in $BaCl_2$-resistant worms included transmembrane potential, anion transport, and cell membrane depolarization, whereas processes such as innervation, long-term synaptic depression, and Na^+ influx co-transport were increased in mean expression (Figure 2A and Tables 1 and S6). Many processes related to the immune system were upregulated, including leukocyte accumulation, leukocyte recruitment, monocyte recruitment, and T cell response (Table 1). Enriched gene networks were involved in both cellular structure and differentiation, as well as cell membrane depolarization confirming transcriptional rewiring of the bioelectric machinery (Table 1). We conclude that $BaCl_2$-adapted heads exhibit transcriptional changes reflective of several subsystems' adaptation to this novel bioelectrical condition and include proteins that could implement physiological homeostasis in response to $BaCl_2$. Tables 1, S4, and S5 and Figure 2A all depict networks for cell processes that were altered in the $BaCl_2$-adapted heads.

To ensure that the RNA-seq identified transcripts that were up- or downregulated in the $BaCl_2$-adapted heads, we performed qPCR. qPCR for *Dj-TRPMa* using primers from (Inoue et al., 2014) showed a 2.4-fold increase in transcripts from $BaCl_2$-adapted heads over WT (Figure 2Ba). qPCR for *Slc2a1* showed a 1.3-fold increase in transcript abundance in $BaCl_2$-adapted heads compared with WT (Figure 2Bb). Although a bit lower in magnitude than reported in the RNA-seq, both showed similar upregulation in $BaCl_2$-adapted heads compared with WT. Thus, despite using a broad platyhelminthes transcriptome, we were able to identify transcripts that were indeed upregulated in $BaCl_2$-adapted heads.

An Excitotoxicity-Based Model of $BaCl_2$-Induced Neural Apoptosis and Adaptation

We next sought to understand the mechanism of $BaCl_2$'s effect and the striking ability of planaria to overcome it with a newly regenerated structure. One plausible explanation for the head degeneration effect is induction of $BaCl_2$-induced drop in resting membrane potential and subsequent neural excitotoxicity in the neuron-rich head of the planarian (Walter et al., 2001, Wright, 2004). Our model is based on the premise that an excitotoxic cascade is initiated by neuronal depolarization induced by the broad potassium channel blocker $BaCl_2$. In other systems, strong depolarization activates V_{mem}-gated Ca^{2+} channels, which causes neurotransmitter exocytosis (Mcmahon and Nicholls, 1993; Sihra et al., 1993). As glutamate signals extracellularly via V_{mem}-depolarizing ionotropic receptors, this further increases cytosolic Ca^{2+}, leading to a positive feedback cycle (see "excitotoxic positive feedback" of Figure 2Cb). We also postulate that disruption of ion balance via $BaCl_2$ should lead to the upregulation of channels and transporters that can help the tissues compensate by breaking positive feedback cycles.

The dynamics of our model under initial $BaCl_2$ exposure and adapted state are shown in Figure 2C. The model makes several specific predictions, shown in Table 2. First, one of the immediate physiological effects of the $BaCl_2$ should be a significant depolarization. Second, manipulation of several components (blockade of calcium channels and chloride channels, activation of dopamine signaling) should prevent the excitotoxicity storm and thus prevent head degeneration due to $BaCl_2$ exposure. Third, blockade of TRPMa channels should counteract the adapted state and lead to head degradation even after adaptation to $BaCl_2$. We thus tested each of these specific predictions in the $BaCl_2$ degeneration and adaptation assay.

Process	Gene Set Seed	# Of Measured Neighbors	Median Change	p Value
Neural/Voltage	Cell membrane depolarization	5	−1.86	0.037
	Cell-cell signaling	10	−1.29	0.036
	Anion transport	17	−1.17	0.049
	Transmembrane potential	85	−1.09	0.032
	Synapse structure	8	1.05	0.019
	Long-term synaptic depression	50	1.16	0.010
	Synaptogenesis	83	1.17	0.045
	Nervous system physiology	26	1.24	0.047
	Neuronal plasticity	46	1.24	0.013
	Transmission of nerve impulse	61	1.28	0.012
	Regulation of action potential	35	1.42	0.005
	Innervation	31	1.88	0.003
	Neuronal guidance	5	2.17	0.033
	Transmembrane signaling	8	2.46	0.012
	Na+ influx co-transport	8	2.99	0.002
	Neurotransmitter uptake	5	3.73	0.019
Immune	T cell response	71	1.04	0.041
	Monocyte recruitment	19	1.42	0.027
	Leukocyte recruitment	25	1.52	0.016
	Leukocyte migration	29	1.58	0.043
	Leukocyte accumulation	12	1.88	0.035
	Neutrophil adhesion	18	1.88	0.042
Other	Melanocyte differentiation	7	−2.44	0.002
	Microtubule depolymerization	9	−2.26	0.011
	Stem cell maintenance	38	−1.20	0.043
	Stem cell proliferation	50	−1.15	0.005
	Melanogenesis	21	1.01	0.047
	Memory	127	1.05	0.036
	Endothelial cell function	54	1.06	0.034
	Intracellular signaling cascade	23	1.24	0.004
	Endothelial cell development	8	1.42	0.021
	Positive chemotaxis	12	2.63	0.029

Table 1. Categories of Transcripts Altered by $BaCl_2$ Adaptation

Differentially expressed cell processes following degeneration and regeneration of a $BaCl_2$-insensitive head, focusing on processes related to membrane potential homeostasis and regeneration. The number of items in the pathway, as well as the median fold change of the network and the p value, is reported for each enriched process. All subnetworks are presented in Table S5.

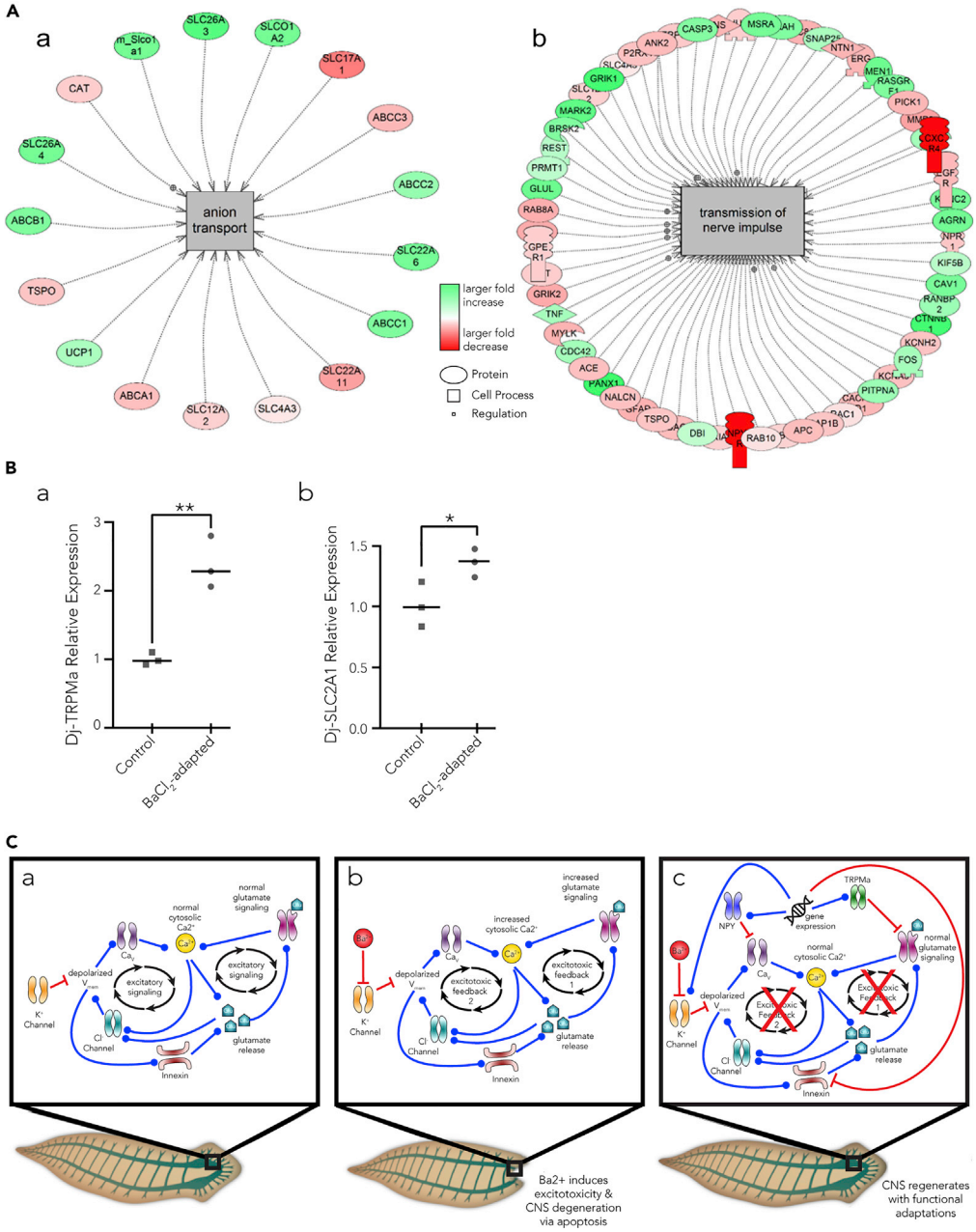

Figure 2. Possible Mechanism of $BaCl_2$-induced Head Degradation Via Excitotoxicity, and Subsequent Adaptation

(A) Pathway Studio v10.0 was used to perform pathway analysis of RNA-seq data for (a) anion transport and (b) transmission of nerve impulse, two pathways critical to deprogression and regeneration of the planaria head. Tables S6A and S6B contain details of all of the components listed here.

(B) qPCR validation of two transcripts identified as upregulated in the RNA-seq—(a) Dj-TRPMa and (b) Slc2a1. Points represent levels for individual worms normalized to GAPDH. Line indicates median. Unpaired t tests were performed to assess significance, $^{**}p < .01$, $^{*}p < .05$, n = 3 for each condition.

(C) Proposed regulatory networks detailing (a) normal/untreated state, (b) the main excitotoxicity-related feedback induced by $BaCl_2$, and (c) proposed adaptations to $BaCl_2$ treatment. Red lines with flat endpoints show an inhibitory/downregulation relationship, whereas blue lines with circular endpoints show an activating/upregulatory relationship. Under normal conditions, K^+ channels hyperpolarize the cell to regulate membrane excitability and therefore maintain an open state of Ca_V channels and upregulate glutamate signaling (a). Ba^{2+} is proposed to induce excitotoxicity in neurons by blocking K^+ channels, leading to significant V_{mem} depolarization, which activates voltage-gated Ca^{2+} channels (Ca_V)

Figure 2. *Continued*

leading to sustained increases in cytosolic Ca^{2+}, excess Ca^{2+}-induced exocytosis of glutamate, and sustained activation of glutamate signaling, leading to further calcium entry to the cell (b, "excitotoxic positive feedback 1"). Ba^{2+}-induced V_{mem} depolarization may also open innexin hemichannels, leading to further glutamate release (b). Extracellular glutamate may activate glutamate-gated chloride channels and increased cytosolic Ca^{2+} may activate Ca^{2+}-gated chloride channels, leading to chloride secretion from cells and further V_{mem} depolarization (b, "excitotoxic positive feedback 2"). Sustained increases in cytosolic Ca^{2+} may initiate apoptosis via caspases, leading to neural degradation (b). Adaptation to Ba^{2+}-induced excitotoxicity is proposed to occur via a variety of changes to gene expression, including upregulation of TRPMa and NPY receptors, which break positive feedback loops supporting excitotoxicity (c).

See also Tables S1, S2–S4, S5, and S6.

Exposure to $BaCl_2$ Results in Depolarization of Anterior Tissues

Although the molecular and cell-level activity of $BaCl_2$ has been thoroughly characterized in *in vitro* preparations (Armstrong and Taylor, 1980; Hanrahan et al., 1986; Kurachi, 1986; Quayle et al., 1988), the effects of $BaCl_2$ exposure on physiological function and/or regeneration *in vivo* are largely unknown. Our excitotoxicity model predicts that $BaCl_2$ should initiate a significant depolarization of the head. To characterize the bioelectric state of the worm after exposure to the potassium channel blocker, we imaged *D. japonica* worms after 30 min in water (Figure 3Aa) and after 30 min in $BaCl_2$ (Figure 3Ab) using the voltage reporter dye $DiBAC_4(3)$, which grows brighter with increasing depolarization. We have previously demonstrated that $DiBAC_4(3)$ is a reliable indicator of depolarization in *D. japonica* (Oviedo et al., 2008; Beane et al., 2011, 2013; Durant et al., 2017, 2019). Figure S1 shows that depolarization with 100 nM of the ionophore valinomycin in combination with 15 mM K^+-gluconate can be visualized in *D. japonica* fragments within an hour of treatment. To compare relative depolarization while minimizing confounding factors, Control and $BaCl_2$-treated worms were mounted and imaged together on the same PIC. After just 30 min in the $BaCl_2$ solution, worms displayed a significant depolarization of anterior tissues (Figure 3Ab, quantified in 3B), as expected from a K^+ channel blocker and predicted by our model. This depolarization was most appreciable in the most anterior 1/6 of the animal. Given the extensive depolarization after just 30 min in $BaCl_2$, we conclude that the robust depolarizing effect of the drug is consistent with our model's prediction.

Calcium and Chloride Blockers Prevent $BaCl_2$-Induced Degeneration

The central component of our model is an excitatory storm and the attendant positive feedback loop involving ion channels and neurotransmitters (Figure 2C). Thus, it predicts that interrupting this loop (inducing neuroprotection) by targeting specific dopamine machinery (Vaarmann et al., 2013; Cepeda et al., 1998; Odaka et al., 2014), chloride channels (Hasbani et al., 1998; Rungta et al., 2015; Takeuchi et al., 2011; Chen et al., 1999), or L-type calcium channels (Szydlowska and Tymianski, 2010; Mark et al., 2001; Hasbani et al., 1998), should prevent degeneration.

To test these predictions, we exposed worms to a combination of $BaCl_2$ and one of several blockers (previously characterized in planaria or other invertebrates), tracking the incidence of degeneration over 3 days and comparing with $BaCl_2$-only controls. All drugs had no effect in the absence of $BaCl_2$ (Figure S2). Since dopamine signaling is both a target of our model and one of the pathways identified by the RNA-seq as altered in the $BaCl_2$-adapted worms (Table S5), we used bromocriptine mesylate (0.5 μM) to activate monoaminergic signaling. Bromocriptine has been shown in mammals to be a dopamine agonist (Liberante et al., 2016; Oda et al., 2008; Parmar et al., 1984; Schneider et al., 1984; Via et al., 2010) but in *D. japonica* appears to have broader functions, agonizing dopaminergic signaling (Chan et al., 2014) and antagonizing serotonergic signaling (Chan et al., 2016). Previous work in *D. japonica* has shown that dopamine and serotonin oppose one another in head regeneration (Chan et al., 2014), indicating that bromocriptine targets general monoaminergic pathways. We hypothesized that bromocriptine would modulate monoaminergic pathways, suppressing excitotoxic activity. We found that bromocriptine was effective at blocking degeneration with 74% of worms experiencing no degeneration until day 2 (Figures 4Ae and 4Af) and 50% of worms experiencing no degeneration up until day 22. Although this effect is noticeable, 38% of the worms did show head degeneration by day 22 and 9% of the worms died during this treatment. Most likely, this failure to protect the worms from degeneration is related to variability in individual worm response to the drug. NPPB (5 μM) and niflumic acid (1.25 μM) were used as calcium-activated chloride channel blockers. Both of these drugs have been shown to block Cl^- channels both in mammalian cells and in *C. elegans* (Bush et al., 2009; Schriever et al., 1999, White and Aylwin, 1990; Wu and Hamill, 1992). NPPB delayed degeneration in most worms (82%) until day 6, at which point all worms died, suggesting only a partial rescue of

Intervention	Reasoning	Experiment
Dopamine signaling agonists (e.g., quinpirole, bromocriptine, cabergoline)	Agonists to dopamine signaling have shown mitigated excitotoxicity (Vaarmann et al., 2013; Cepeda et al., 1998; Odaka et al., 2014)	Dopamine agonist and serotonin 5-HT_7-like receptor antagonist bromocriptine significantly delayed head degeneration in the majority of worms for the duration of the test (35 days) compared with control, which showed full degeneration within 24 h (Figures 4Ae and 4Af)
Cl^- channel inhibitors	Previous studies have shown decreased neural death during excitotoxic cascades in the presence of chloride channel antagonists (Inoue et al., 2007; Chen et al., 1998; Rungta et al., 2015; Liang et al., 2007)	Chloride channel blockers NPPB and NFA significantly delayed head degeneration upon exposure to $BaCl_2$. 12% of NPPB- and 17% of NFA-treated worms showed some degeneration by day 3 compared with 100% of controls (Figures 4Ag–4Aj)
Calcium channel antagonists	Excitotoxicity is mediated by high intracellular Ca^{2+} levels, a component of which arises from neuronal voltage-gated Ca^{2+} channels (Lai et al., 2014; Szydlowska and Tymianski, 2010). And calcium channel antagonists can prevent neuronal death (Prentice et al., 2015)	L-type calcium channel blocker Nicardipine delayed degeneration in 69% of worms (31% showed some degeneration) through 3 days of treatment compared with 100% degeneration in controls (Figures 4Ak and 4Al)
TRPM antagonists	TRP channels show complex involvement in excitotoxicity (Szydlowska and Tymianski, 2010; Zheng and Phelan, 2014; Aarts and Tymianski, 2005; Bengtson et al., 2004; Li et al., 2012). We found that a TRPM channel is significantly upregulated in Ba^{2+}-adapted regenerated heads (Table 3A), suggesting TRPM inhibition may sabotage the mechanism by which planaria adapt to $BaCl_2$	TRPM antagonist AMTB leads to rapid (less than 24 h) head degeneration in $BaCl_2$-adapted worms, whereas adapted worms maintained in $BaCl_2$ did not degenerate (Figure 4B)

Table 2. Summary of Targets Predicted from $BaCl_2$-Induced Excitotoxicity Hypothesis and the Results of Experimental Interventions

the excitotoxic effect (Figures 4Ag and 4Ah). Niflumic acid, on the other hand, was able to prevent head degeneration or death up until day 2 in 92% of the treated planaria but did occasionally induce ectopic eyes (1.9%) (Figures 4Ai and 4Aj). Finally, nicardipine hydrochloride (2.5 μM) was used to block L-type calcium channels (Beane et al., 2011; Hockerman et al., 1997; Mendonca-Silva et al., 2006; Nogi et al., 2009). Nicardipine induced a delay in degeneration in 78% of worms through 2 days of treatment (Figures 4Ak and 4Al). Taken as a whole, exposure to these channel activity modifiers similarly prevented $BaCl_2$-mediated head degeneration (Figure 4A, quantified in 4Am) and mostly also prevented $BaCl_2$-induced death in the planaria, suggesting that these drugs directly acted on the mechanism by which $BaCl_2$ is toxic. We conclude that, as predicted by our model, drugs predicted to break the positive feedback loop of excitotoxicity efficiently suppress the $BaCl_2$-induced head deprogression.

Blocking Adaptation

Conversely, we next asked whether our model also suggested efficacious methods of counteracting the $BaCl_2$-adapted state. A transcript identified at significant levels only in the $BaCl_2$-adapted heads

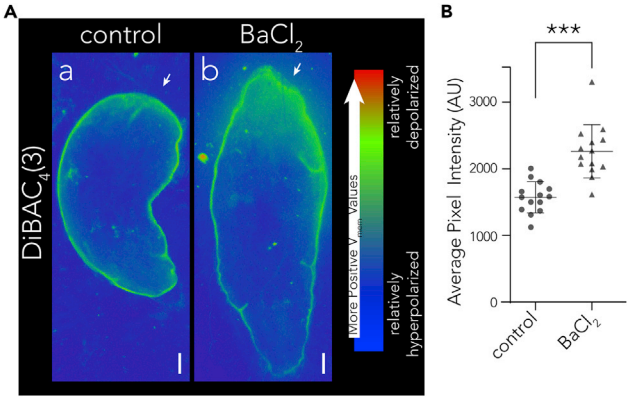

Figure 3. Visualization of Relative Membrane Potential in WT and $BaCl_2$-treated *D. japonica* Flatworms

(A) Voltage-sensitive dye was used to determine pattern of resting potentials in planaria. White arrowheads indicate the anterior of the worm. Images are pseudocolored to allow for ease of visualization of depolarization patterns, but worms were imaged in the same frame so as not to confound data after pseudocoloring, and all image analysis was done using raw un-colored images. (a) Untreated *D. japonica* flatworm imaged with $DiBAC_4(3)$ dye. (b) *D. japonica* flatworm imaged with $DiBAC_4(3)$ dye after 30 min in $BaCl_2$. Scale bars, 0.5 mm.

(B) Quantification of average pixel intensities in untreated and $BaCl_2$-treated worms. Bars represent mean ± SD. Welch's unpaired t test, ***p = 0.00002.

See also Figure S1.

(Table 3) was *TRPMa*–a member of a family of channels that sense chemical, mechanical, and osmotic signals (opening with cell swelling) and convey signals to the genome via increased intracellular Ca^{2+}. Thus, we next blocked TRPM via the well-characterized TRPM blocker AMTB (Lashinger et al., 2008, Yapa et al., 2018), which has previously been shown (and confirmed by RNAi) to be effective in inhibiting TRPMa in planaria (Inoue et al., 2014). Although exposure to 100 μM AMTB alone did not induce any head degeneration or death (Figure 4Bb), $BaCl_2$-adapted planaria began degenerating their heads after just an hour and a half of exposure to AMTB (24 h time point shown in Figure 4Bd). By 24 h of exposure, 98% of heads had fully degenerated, whereas worms that were maintained in $BaCl_2$ showed no degeneration (Figure 4Bc). This rate of degeneration is equivalent to the controls that had never experienced $BaCl_2$ adaptation (Figures 1Aa, 4Aa, and 4Ab). Furthermore, in the presence of both $BaCl_2$ and AMTB, 62% of the planaria died within 48 h, suggesting that the mechanism by which they adapted to the $BaCl_2$ could not overcome both $BaCl_2$ and AMTB. Thus, we conclude that, consistent with the known mechanisms of excitotoxicity, $BaCl_2$ adaptation can be erased by TRPM blockade.

DISCUSSION

Planarian Regeneration Can Compensate for Dramatic Physiological Perturbations

Habituation to extreme physiological stressors has been known since the classic experiments of Jollos, who showed that lineages of paramecia exposed to toxins or extreme heat gained resistance that persisted for hundreds of generations (Jollos, 1933, 1934). However, very little information is available on the mechanism of such plasticity taking place in single organisms (i.e., not due to multi-generational selection) (Elgart et al., 2015). Here we established a model for studying the interplay of physiological and transcriptional plasticity on a short timescale. The planarian head degeneration model also has the advantage that it reveals a multi-scale phenomenon: the cellular stress must be coupled to organism-wide patterning networks, as the animal has to rebuild a complex new structure that will maintain its anatomical integrity while the cells within are forced to significantly alter their normal physiological function.

As a model system, we chose planaria because of their remarkable ability to regulate anatomy despite drastic injury (Saló et al., 2009; Owlarn and Bartscherer, 2016), targeting the function of K^+ channels, as these are required for a wide range of processes at the level of cell behavior (Urrego et al., 2014; Pardo and Stuhmer, 2014) and body-wide patterning (Adams et al., 2016; Dahal et al., 2012; Simons et al., 2015; Masotti et al., 2015). Bioelectric processes underlie behavioral plasticity in the brain, suggesting

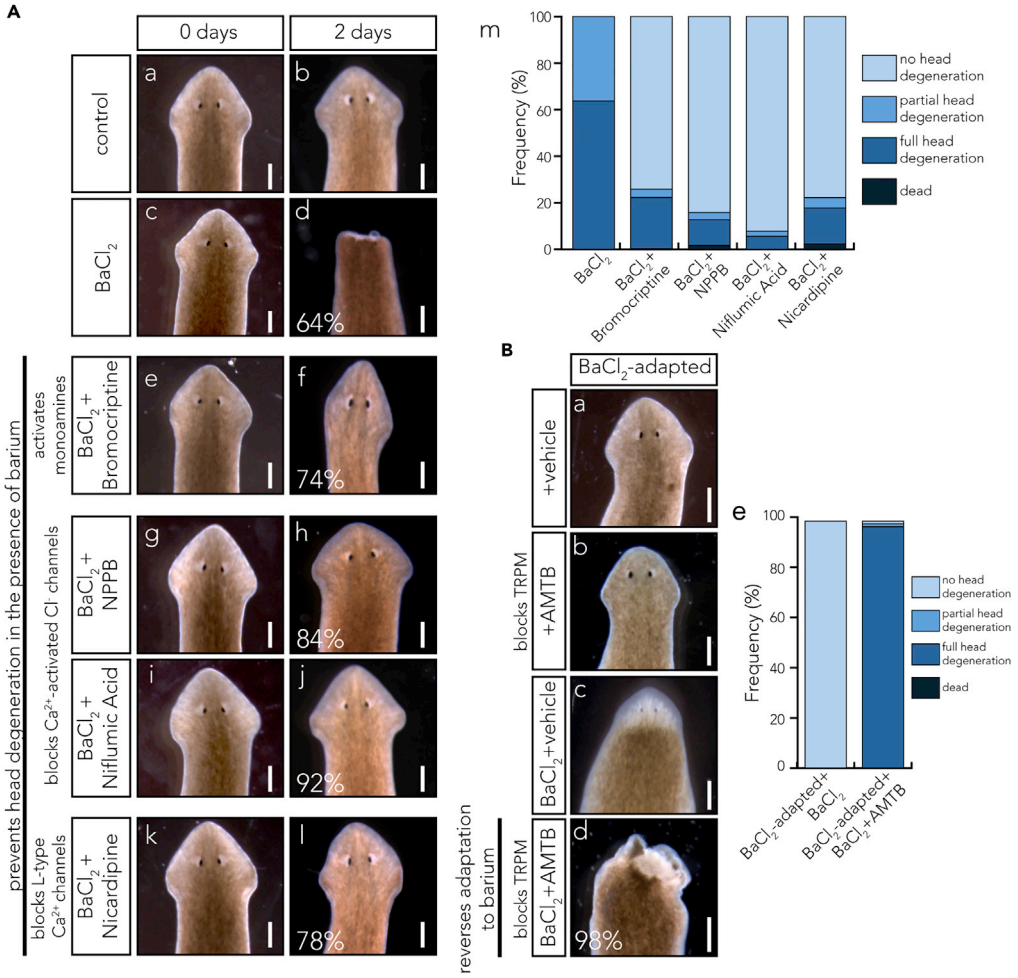

Figure 4. Targeting Ion Channels Allows Modulation of Degeneration and Adaptation

(A) A variety of drugs targeting ion channels were used to test our excitotoxicity hypothesis. (a and b) *D. japonica* worm before treatment (a) and after 2 days in water (b). (c and d) Planaria treated with 1 mM $BaCl_2$ for 0 h (c) show no phenotype, but after 48 h, the head deprogresses (d). (e and f) Planaria in dopamine agonist bromocriptine (0.5 μM) and 1 mM $BaCl_2$ solution for 0 (e) and 2 days (f). Bromocriptine is able to prevent head degeneration upon exposure to $BaCl_2$ in 74% of worms (f). (g) exposure to $BaCl_2$ and calcium-activated chloride channel blocker NPPB (5 μM) has no effect at the time of treatment, but within 2 days (h) NPPB has prevented head degeneration in 84% of worms. (i and j) Calcium-activated chloride channel blocker Niflumic acid (1.24 μM) exposure in combination with $BaCl_2$ has no effect at 0 days (i) but prevents head degeneration in 92% of worms within 2 days (j). (k and l) L-type calcium channel blocker nicardipine hydrochloride (2.5 μM) treatment in combination with $BaCl_2$ has no effect at the time of treatment (k) but prevents head degeneration in 78% of worms within 2 days (l). Scale bars, 0.5 mm. (m) Prevalence of head degeneration phenotype with each of the drug treatments listed in (e–l). The overwhelming majority of worms with head degeneration in the $BaCl_2$-treated worms are replaced with the majority of worms not experiencing head degeneration when treated with ion channel modulators.

(B) Resensitization of worms to $BaCl_2$. $BaCl_2$-adapted *D. japonica* worms in (a) water, (b) water with 100 μM AMTB hydrochloride, or (c) water with $BaCl_2$ do not induce head degeneration in $BaCl_2$-adapted worms. (d) However, treatment with AMTB (100 μM) in addition to further treatment with $BaCl_2$ induced head degeneration within 1.5 h. Scale bars, 0.5 mm. (e) Prevalence of head degeneration phenotypes in $BaCl_2$-adapted, $BaCl_2$-treated planaria with or without AMTB treatment, as shown in (c) and (d). Treatment with AMTB resulted in a near-complete change from normal heads to fully degenerated heads.

See also Figure S2.

the hypothesis that ionic mechanisms may be of considerable interest in understanding different kinds of adaptation (Pezzulo and Levin, 2015). Interestingly, recent work in *Drosophila* mutants revealed the importance of regulation of excitability to buffer against environmental changes (Kim et al., 2017).

Protein Name	TCONS	Gene Name	Log Fold Change	p Value	q Value
Metalloendopeptidase (EC 3.4.24.-)	TCONS_00013146	NA	–	p < 0.001	0.004
Voltage-gated potassium channel	TCONS_00008343	NA	–	p < 0.001	0.020
Palmitoyltransferase (EC 2.3.1.225)	TCONS_00010738	CLF_106085	–	p < 0.001	0.022
GCR085	TCONS_00007438	gcr085	–	0.001	0.027
Transient receptor potential ion channel Ma DjTRPMa (fragment)	TCONS_00000400	NA	–	0.001	0.030
Slc17a-1 (Vesicular glutamate transporter)	TCONS_00006778	vglut slc17a-1	–	0.001	0.030
NPYR-14 (Neuropeptide Y receptor)	TCONS_00002461	npyr-14	–	0.001	0.031
Neuroglian	TCONS_00013039	EGR_00,245	–	0.001	0.031
Ubiquitin thioesterase (EC 3.4.19.12)	TCONS_00004623	NA	–	0.001	0.040
Slc2a-1 (Glut1, glucose transporter)	TCONS_00003196	slc2a-1	3.11838	0.001	0.030
SMED-SMAD6/7-2	TCONS_00000433	NA	2.31825	0.002	0.050
Clone ZZD1463 mRNA sequence (Rab-protein 8)	TCONS_00005887	Rab8	2.12996	p < 0.001	0.004
Aquaporin	TCONS_00007316	aquaporin	2.01898	p < 0.001	0.004

Table 3. Summary of Transcripts Upregulated in Heads Pre-Conditioned by $BaCl_2$ Exposure

Transcripts with greater than a 2-fold change in expression, significance of $q < 0.05$, with clear annotation are shown. A log fold change of "–" indicates transcripts that were only identified in $BaCl_2$-treated worms and thus have no calculatable fold change. Bolded transcripts are associated with our excitotoxicity model. TCONS refers to the transcript ID in Table S1.

Upon exposure to $BaCl_2$, a potent non-specific K^+ channel blocker, planaria experience a striking degradation of the entire head. Remarkably, they are then able to produce a new head that is insensitive to the $BaCl_2$ (Figure 1A). We characterized this example of large-scale adaptation to a drastic physiological challenge by regenerative processes.

Extended Time in Water Results in a Loss of $BaCl_2$ Resistance

The acquired resistance to $BaCl_2$ is not permanent. When $BaCl_2$-insensitive worms are placed in water for 30 days, they lose their resistance to $BaCl_2$, and upon a second exposure to $BaCl_2$ will undergo degeneration and regeneration of anterior tissues again (Figure 1B). Interestingly, 30 days is approximately the time required for cellular turnover in planaria (Pellettieri and Sánchez Alvarado, 2007); it is not known yet whether the $BaCl_2$ adaptation and de-adaptation is in some way tied to the temporal profile of neoblast activity and somatic cell turnover. Taken together, this temporal profile of adjustment to novel stimuli, and its return to normal, highlights the ability of living systems to adaptively, flexibly integrate information from the internal and external environments of the organism via the interplay between physiological information and genetic programs. The fact that $BaCl_2$ adaptation spontaneously reverses suggests that the adapted state is not a stable attractor in the transcriptional landscape (Huang et al., 2005; Sullivan et al., 2016); instead, it is compatible with a dynamic monitoring system that adjusts to novel stressors but can also detect their cessation. Future development of transgenic strains of planaria expressing novel physiological fluorescent

reporters will be invaluable in tracing the exact temporal profiles of signaling cascades during this process *in vivo*.

$BaCl_2$ Adaptation Involves a Unique Transcriptional Signature

To investigate the mechanism of head degeneration and subsequent $BaCl_2$ tolerance, we analyzed transcriptomes comparing WT heads with $BaCl_2$-adapted heads. Importantly, we analyzed completely regenerated heads, so that the profiles would reflect not mechanisms involved in head regeneration per se, but differences in mature normal and $BaCl_2$-insensitive heads. RNA-seq analysis revealed a number of transcriptional differences that distinguish WT ($BaCl_2$-sensitive) heads from $BaCl_2$-adapted heads (Tables 3 and S1). Unfortunately, no gain-of-function technology exists in planaria that can be used to misexpress transcripts; however, we exploited the druggable nature of some of the key targets to individually modulate both the degeneration and adaptation phases (Figure 4). It must be noted that important changes can occur at the level of physiology, not transcription, and it is likely that additional mechanisms of plasticity that are invisible to RNA-seq remain to be characterized in future work.

Transcriptional Rewiring of Bioelectric Networks

One of the most salient aspects of the RNA-seq dataset was the identification of changes in genes involved in regulating bioelectric state (Table 1). Overall, 1.98% of the transcripts identified by RNA-seq in planaria were affected by $BaCl_2$ exposure ($q < 0.05$, >2-fold change). A number of channels and pumps are altered in the transition from $BaCl_2$ sensitivity to adaptation, including calcium-sensitive transporters, solute transporters, voltage-gated channels, and others (Tables S1, 1, and 3). Interestingly, many of these channels are transporters, suggesting that the physiological buffering of a depolarizing treatment is dependent on employing alternative means of transporting ions into and out of anterior cells and tissues. Newly developed platforms for bioelectric simulation will enable construction and analysis of quantitative physiological models linking post-translational ion flow dynamics (channel opening/closing) to transcriptional regulation and may explain how the observed changes in the electrogenic mRNA profile can compensate for $BaCl_2$ exposure (Pietak and Levin, 2016; Cervera et al., 2015, 2016a, 2016b). Future functional analysis will also investigate physiological repercussions of detected transcriptional changes.

An Excitotoxicity Model of Degeneration and Adaptation

To understand this striking phenomenon, we formulated and tested a model based on excitotoxicity (Mark et al., 2001; Szydlowska and Tymianski, 2010). We propose that depolarized V_{mem} resulting from Ba^{2+} block of K^+ channels (Walter et al., 2001), as well as the Ba^{2+} ion's ability to substitute for Ca^{2+} in a variety of processes (Condrescu et al., 1997, Dingledine et al., 1992, Zhou et al., 2012; Ni et al., 2014), induces glutamate-mediated excitotoxicity (Figure 2C). It was hypothesized that Ba^{2+} induces a strong depolarization of V_{mem} by blocking K^+ channels (Wright, 2004; Walter et al., 2001), which in turn activates voltage-gated Ca^{2+} channels, leading to increases in both intracellular Ca^{2+} and potentially Ba^{2+} (Mark et al., 2001; Szydlowska and Tymianski, 2010). Increased Ca^{2+} and Ba^{2+} then induce glutamate exocytosis, which may signal at ionotropic glutamate receptors to further depolarize V_{mem} and increase cytosolic Ca^{2+} and Ba^{2+} in positive feedback (Mcmahon and Nicholls, 1993, Sihra et al., 1993; Mark et al., 2001; Lau and Tymianski, 2010), leading to an excitotoxic cascade and neural death via Ca^{2+} activation of apoptosis (Zhang and Bhavnani, 2005; Mcmahon and Nicholls, 1993). One of the key predictions of our model is that a strong anterior depolarization should be present early in the process, which was indeed observed (Figure 3).

Remarkably, the organism is able to alter its transcriptional profile to regenerate new heads that are resistant to $BaCl_2$. Neuroprotective changes in $BaCl_2$-adapted heads include increased expression of neuropeptide Y receptors and dramatically decreased expression of innexins (invertebrate gap junctions), both of which have been previously shown to inhibit glutamate-induced excitotoxicity. Increased NPY signaling has been found to modulate excitotoxicity (Greber et al., 1994; Grundemar et al., 1991a, 1991b; Whittaker et al., 1999; Silva et al., 2005) and may act through inhibition of Ca^{2+} channels (Grundemar et al., 1991a, Mccullough et al., 1998). Past work in numerous systems has shown a strong neuroprotective effect of gap junction blockade in excitotoxic cascades, where gap junction inhibition has shown significant reduction in neural death (Wang et al., 2010, 2012; Galinsky et al., 2017; Takeuchi et al., 2011; Thompson, 2015; Belousov et al., 2017). Other changes include increased expression of a TRPM channel, increased aquaporin channels, and increased levels of a voltage-gated K^+ channel, which appear to convey neuroprotective adaptations to the regenerated heads. Decreases in glutamine transporter *Slc38a2* (which increases neural glutamate via the glutamine-glutamate cycle [Bak et al., 2006]) were also found. These findings

reveal the transcription-level acquisition of tolerance to a significant toxic challenge by planarian regeneration. Additional adaptive changes, at the protein or physiological levels, may also have occurred and will be studied in subsequent work.

Ion Channels' Roles in Degeneration and Adaptation

Our model implicated specific classes of targets in the degeneration and adaptation process. Indeed, we found that blockade of calcium and chloride channels were able to counteract the toxic effects of $BaCl_2$ exposure (Figures 4Ag–4Al). Likewise, monoaminergic activation was also able to prevent degeneration (Figures 4Ae and 4Af). These results demonstrate that an adaptive stress response ($BaCl_2$ insensitivity) can be artificially induced without prior exposure to the actual stressor. Importantly, our model also enabled identification of a simple intervention to reverse the adapted state—TRPMa channel blockers rapidly induced $BaCl_2$-sensitivity to $BaCl_2$-adapted heads (Figure 4B), revealing the induction of TRPMa after $BaCl_2$ exposure as a key functional step in the observed regenerative plasticity. Although any pharmacological reagent may have additional targets, the use of several diverse channel drugs to cleanly abrogate a very specific process, and improve tissue health and integrity (i.e., not simply cause toxicity), supports the predictive value of our model. Any future models of this process can likewise be evaluated by their ability to identify reagents that enable modulation of the plasticity process. The use of small molecule drugs to target these kinds of processes *in vivo* is an important complement to genetic manipulation studies, as it may allow therapeutic applications that do not require gene therapy. Targeting both phases of the adaptive response (the initial toxicity and the resulting adapted state), as shown in our data, represents an important strategy in applications.

Conclusion

Planaria are champions of plasticity and robustness, not only repairing their anatomy after amputation in normal conditions, but also apparently able to adjust their physiology to survive and regenerate under significant physiological perturbation. This occurs within an individual's lifetime, not via population selection, revealing the ability of tissues to activate appropriate responses to relieve physiological stressors. Using this and similar tractable models will allow a better understanding of the dynamics of biological circuits, not only hardwired activity emergent from genetically encoded features, but also flexible adaptation to unpredictable stimuli. The study of the mechanisms and algorithms that enable this property blurs the line between developmental genetics, adult physiology, and the kind of plasticity studied in neuroscience. Interestingly, our NGS analysis implicated targets belonging to the Memory/Neuroplasticity categories (Table 1), suggesting the hypothesis, which we will test in future work, that regenerative and physiological plasticity are related to (and perhaps early forms of) cognitive plasticity in higher animals (Baluška and Levin, 2016).

We chose $BaCl_2$ for two reasons. First, because as a very broad K^+ channel blocker, it would challenge tissues with a stress that could not easily be overcome through simple redundancy among potassium channel family members. Second, because to our knowledge, exposure to significant quantities of $BaCl_2$ is not something planaria encounter in the wild. Thus, it is plausible that plasticity to $BaCl_2$ toxicity is not a genetic response that has been specifically selected for; rather than a hardwired response to a common feature of the planarian environment over evolutionary time, it is likely that the remarkable adaptation we observe is an example of a more general and still poorly understood feature of biology: robustness in the face of novel stresses. The algorithms and mechanisms by which living systems match transcriptional and physiological responses to environmental challenges represent a key intellectual challenge for the coming decade, with significant implications both for biomedicine and for the design of highly resilient systems in engineering.

Understanding cellular adaptation to stress may have implications in addition to shedding light on evolvability and regulative morphogenesis. Although other species may not exhibit the convenient head degeneration phenotype, ionic disbalance and stress response is a universal biological and biomedical phenomenon. Moreover, preconditioning (exposure to preinjury stressors to achieve induction of tolerance) (Yokobori et al., 2013) is an important topic in the biomedicine of brain injury and epilepsy (Blondeau et al., 2000; Fern et al., 2014), where ion channels are already beginning to be viewed as therapeutic targets for neuroprotection (Skaper, 2011). Future work on the modulation of regeneration via developmental pharmacology will exploit novel biomaterials, computational models, and ion channel drugs to transition these advances toward biomedical applications (Herrera-Rincon et al., 2018; Churchill et al., 2018; Pai et al., 2018).

Protein Name	TCONS	Gene Name	Log Fold Change	p Value	q Value
Tubulin alpha chain (fragment)	TCONS_00000293	TBA3 TR27993	–	p < 0.001	0.004
Marvel containing potential lipid	TCONS_00001520	EgrG_000088200	–	p < 0.001	0.004
GCR041	TCONS_00002574	gcr041	–	p < 0.001	0.004
Propionyl-CoA synthetase	TCONS_00010061	CLF_100045	–	p < 0.001	0.004
Propionyl-CoA synthetase	TCONS_00010062	CLF_100045	–	p < 0.001	0.004
cAMP-dependent protein kinase regulatory subunit	TCONS_00014767	PRKAR2A	–	p < 0.001	0.004
CyclinA-like protein (fragment)	TCONS_00014792	NA	–	p < 0.001	0.004
Tubulin alpha chain	TCONS_00000293	NA	–	p < 0.001	0.004
Uncharacterized protein C1orf177 homolog	TCONS_00015160	CA177 TR105569	–	p < 0.001	0.004
Fibronectin type 3 and ankyrin repeat domains protein 1 (FANK1)	TCONS_00015183	CLF_102920	–	p < 0.001	0.004
Mariner Mos1 transposase	TCONS_00015672	HmN_000702600	–	p < 0.001	0.004
Tubulin alpha chain	TCONS_00015804	NA	–	p < 0.001	0.004
L-lactate dehydrogenase (EC 1.1.1.27)	TCONS_00014875	NA	–	p < 0.001	0.007
TBC1 domain family member 9B	TCONS_00012203	CLF_111893	–	0.001	0.031
SPSB	TCONS_00002395	Spsb	−8.9764	p < 0.001	0.004
SPSB	TCONS_00015862	Spsb	−6.74196	p < 0.001	0.004
Slc38a-2 (Na+-coupled neutral amino acid transporter)	TCONS_00008866	slc38a-2	−5.10772	p < 0.001	0.004
Tubulin alpha chain	TCONS_00000243	MS3_11,213	−5.00986	p < 0.001	0.004
Tubulin beta chain	TCONS_00015047	TR83001	−4.80567	p < 0.001	0.043
Tubulin beta chain	TCONS_00015847	NA	−4.02875	p < 0.001	0.004
Tubulin alpha chain	TCONS_00014885	NA	−3.9266	p < 0.001	0.004
C3H-zinc finger-containing protein 1	TCONS_00015349	NA	−3.87679	p < 0.001	0.004
Phosphotransferase (EC 2.7.1.-)	TCONS_00015828	slc25a-4	−3.86765	p < 0.001	0.004
Y box protein 4-like protein	TCONS_00000137	NA	−3.65495	p < 0.001	0.004
Protein FAM154A	TCONS_00015465	EmuJ_000818000	−3.60524	p < 0.001	0.004
Plastin-1	TCONS_00015023	CLF_110637	−3.56204	p < 0.001	0.016
Innexin	TCONS_00005338	**inx**	**−3.54459**	p < 0.001	**0.004**
Tubulin beta chain	TCONS_00000701	NA	−3.41177	p < 0.001	0.004
Tubulin beta-2C chain	TCONS_00000158	NA	−3.37944	p < 0.001	0.004
SJCHGC04177 protein	TCONS_00015105	NA	−3.37057	p < 0.001	0.004
Tubulin alpha chain (fragment)	TCONS_00015786	CLF_103359	−3.25329	p < 0.001	0.004
Tubulin beta chain (fragment)	TCONS_00002700	bt3	−3.05291	p < 0.001	0.004
Expressed conserved protein	TCONS_00014926	EmuJ_001095400	−2.98249	p < 0.001	0.004

Table 4. Summary of Transcripts Downregulated in Heads Pre-Conditioned by $BaCl_2$ Exposure

(Continued on next page)

Protein Name	TCONS	Gene Name	Log Fold Change	p Value	q Value
Tubulin alpha chain	TCONS_00014888	NA	−2.83912	0.001	0.034
T-complex protein 1 subunit gamma (fragment)	TCONS_00015722	T265_13,906	−2.74806	p < 0.001	0.013
C3H-zinc finger-containing protein 1	TCONS_00015007	NA	−2.74023	p < 0.001	0.007
Plasminogen-1 (fragment)	TCONS_00014024	NA	−2.66561	p < 0.001	0.004
SJCHGC05018 protein	TCONS_00000671	NA	−2.65743	p < 0.001	0.004
Tubulin alpha chain (fragment)	TCONS_00000134	atub2	−2.34531	p < 0.001	0.004
Tubulin alpha chain	TCONS_00014770	NA	−2.19894	p < 0.001	0.024
Trypsin-like serine protease	TCONS_00009159	NA	−1.9831	p < 0.001	0.004

Table 4. *Continued*

Transcripts significantly downregulated by $BaCl_2$ treatment with greater than a 2-fold change in expression, significance of $q < 0.05$, with clear identification are shown. A log fold change of "–" indicates transcripts that were only identified in untreated worms and thus have no calculatable fold change. Bolded transcripts are specifically predicted by our excitotoxicity model. TCONS refers to the transcript ID in Table S1.

Limitations of the Study

One of the limitations of the study is that assays are not yet available in planaria to directly observe the physiological effects of all of the reagents used. Most of the pharmacological tools we applied have been used in planaria, and all have been utilized in other invertebrates, but NPPB and Niflumic acid have not heretofore been characterized in planaria. Likewise, there is currently no working technology for introducing foreign genes into planaria, preventing the use of molecular-genetic (dominant negative and fluorescent reporter) tools to directly observe the dynamics of the dopamine pathway under our various conditions. Furthermore, it is possible that some of the genes listed in Tables 3 and 4 as expressed in one condition but not detected in the other may reflect technical or statistical failures to detect transcript. Finally, it will be important in future work to conduct a large-scale RNAi effort targeting all of the genes identified by our RNA-seq to determine whether additional mechanisms of tissue adaptation to stress are also critical beyond those implicated in the specific model we propose.

METHODS

All methods can be found in the accompanying Transparent Methods supplemental file.

SUPPLEMENTAL INFORMATION

Supplemental Information can be found online at https://doi.org/10.1016/j.isci.2019.11.014.

ACKNOWLEDGMENTS

We thank the members of the Levin lab and Nicolas Roleau for useful discussions and Hans Gonzembach and the diligent undergraduates including Hannah Stowe, Quynh Anh Phan, Si Kun Wang, Sara E. Mitchell, Tien Hoang, John Fernandez, and Carolyn H. Nguyen who have helped us tend to our worm colony. We also thank members of the Agata lab for providing us with the *Dj-TRPMa* primer sequences. We gratefully acknowledge support by an Allen Discovery Center award from the Paul G. Allen Frontiers Group (No. 12171), the Templeton World Charity Foundation (No. TWCF0089/AB55), and the Barton Family Foundation. Research was sponsored by the Defense Advanced Research Projects Agency (DARPA) under Cooperative Agreement Number HR0011-18-2-0022. The content of the information does not necessarily reflect the position or the policy of the Government, and no official endorsement should be inferred. Approved for public release; distribution is unlimited.

AUTHOR CONTRIBUTIONS

M.L. and M.E.-B. conceived and planned the study. M.E.-B., F.D., A.T., D.D., and J.M. performed planarian experiments and analyzed data. K.M., A.T., and D.D. performed molecular biology (QPCR validation). A.P.

built and analyzed the excitotoxicity model. C.J.M. and A.K. analyzed RNA-seq data. M.E.-B, A.K., A.P., and M.L. wrote the paper.

DECLARATION OF INTERESTS

The authors declare no competing interests.

Received: May 21, 2019
Revised: October 1, 2019
Accepted: November 5, 2019
Published: December 20, 2019

REFERENCES

Aarts, M.M., and Tymianski, M. (2005). TRPMs and neuronal cell death. Pflugers Arch. *451*, 243–249.

Adams, D.S., Uzel, S.G., Akagi, J., Wlodkowic, D., Andreeva, V., Yelick, P.C., Devitt-Lee, A., Pare, J.F., and Levin, M. (2016). Bioelectric signalling via potassium channels: a mechanism for craniofacial dysmorphogenesis in KCNJ2-associated Andersen-Tawil Syndrome. J. Physiol. *594*, 3245–3270.

Armstrong, C.M., and Taylor, S.R. (1980). Interaction of barium ions with potassium channels in squid giant axons. Biophys. J. *30*, 473–488.

Bak, L.K., Schousboe, A., and Waagepetersen, H.S. (2006). The glutamate/GABA-glutamine cycle: aspects of transport, neurotransmitter homeostasis and ammonia transfer. J. Neurochem. *98*, 641–653.

Balaban, N.Q., Merrin, J., Chait, R., Kowalik, L., and Leibler, S. (2004). Bacterial persistence as a phenotypic switch. Science *305*, 1622–1625.

Baluška, F., and Levin, M. (2016). On having No head: cognition throughout biological systems. Front. Psychol. *7*, 902.

Beane, W.S., Morokuma, J., Adams, D.S., and Levin, M. (2011). A Chemical genetics approach reveals H,K-ATPase-mediated membrane voltage is required for planarian head regeneration. Chem. Biol. *18*, 77–89.

Beane, W.S., Morokuma, J., Lemire, J.M., and Levin, M. (2013). Bioelectric signaling regulates head and organ size during planarian regeneration. Development *140*, 313–322.

Belousov, A.B., Fontes, J.D., Freitas-Andrade, M., and Naus, C.C. (2017). Gap junctions and hemichannels: communicating cell death in neurodevelopment and disease. BMC Cell Biol. *18*, 4.

Bengtson, C.P., Tozzi, A., Bernardi, G., and Mercuri, N.B. (2004). Transient receptor potential-like channels mediate metabotropic glutamate receptor EPSCs in rat dopamine neurones. J. Physiol. *555*, 323–330.

Blondeau, N., Plamondon, H., Richelme, C., Heurteaux, C., and Lazdunski, M. (2000). K(ATP) channel openers, adenosine agonists and epileptic preconditioning are stress signals inducing hippocampal neuroprotection. Neuroscience *100*, 465–474.

Brunke, S., and Hube, B. (2014). Adaptive prediction as a strategy in microbial infections. PLoS Pathog. *10*, e1004356.

Bush, E., Foreman, R., Walker, R.J., and Holden-Dye, L. (2009). The actions of chloride channel blockers, barbiturates and a benzodiazepine on *Caenorhabditis elegans* glutamate- and ivermectin-gated chloride channel subunits expressed in *Xenopus* oocytes. Invert. Neurosci. *9*, 175–184.

Cebrià, F., Adell, T., and Saló, E. (2018). Rebuilding a planarian: from early signaling to final shape. Int. J. Dev. Biol. *62*, 537–550.

Cepeda, C., Colwell, C.S., Itri, J.N., Gruen, E., and Levine, M.S. (1998). Dopaminergic modulation of early signs of excitotoxicity in visualized rat neostriatal neurons. Eur. J. Neurosci. *10*, 3491–3497.

Cervera, J., Manzanares, J.A., and Mafe, S. (2015). Electrical coupling in ensembles of nonexcitable cells: modeling the spatial map of single cell potentials. J. Phys. Chem. B *119*, 2968–2978.

Cervera, J., Alcaraz, A., and Mafe, S. (2016a). Bioelectrical signals and ion channels in the modeling of multicellular patterns and cancer biophysics. Sci. Rep. *6*, 20403.

Cervera, J., Meseguer, S., and Mafe, S. (2016b). The interplay between genetic and bioelectrical signaling permits a spatial regionalisation of membrane potentials in model multicellular ensembles. Sci. Rep. *6*, 35201.

Chan, J.D., Agbedanu, P.N., Zamanian, M., Gruba, S.M., Haynes, C.L., Day, T.A., and Marchant, J.S. (2014). 'Death and axes': unexpected Ca(2+) entry phenologs predict new anti-schistosomal agents. PLoS Pathog. *10*, e1003942.

Chan, J.D., Grab, T., and Marchant, J.S. (2016). Kinetic profiling an abundantly expressed planarian serotonergic GPCR identifies bromocriptine as a perdurant antagonist. Int. J. Parasitol. Drugs Drug Resist. *6*, 356–363.

Chen, Q., Olney, J.W., Lukasiewicz, P.D., Almli, T., and Romano, C. (1998). Ca2+-independent excitotoxic neurodegeneration in isolated retina, an intact neural net: a role for Cl- and inhibitory transmitters. Mol. Pharmacol. *53*, 564–572.

Chen, Q., Moulder, K., Tenkova, T., Hardy, K., Olney, J.W., and Romano, C. (1999). Excitotoxic cell death dependent on inhibitory receptor activation. Exp. Neurol. *160*, 215–225.

Churchill, C.D.M., Winter, P., Tuszynski, J.A., and Levin, M. (2018). EDEn – electroceutical design environment: an ion channel database with small molecule modulators and tissue expression information. iScience *11*, 42–56.

Condrescu, M., Chernaya, G., Kalaria, V., and Reeves, J.P. (1997). Barium influx mediated by the cardiac sodium-calcium exchanger in transfected Chinese hamster ovary cells. J. Gen. Physiol. *109*, 41–51.

Cooke, J. (1981). Scale of body pattern adjusts to available cell number in amphibian embryos. Nature *290*, 775–778.

Corning, W.C., and Freed, S. (1968). Planarian behaviour and biochemistry. Nature *219*, 1227–1229.

Dahal, G.R., Rawson, J., Gassaway, B., Kwok, B., Tong, Y., Ptacek, L.J., and Bates, E. (2012). An inwardly rectifying K+ channel is required for patterning. Development *139*, 3653–3664.

Dingledine, R., Hume, R.I., and Heinemann, S.F. (1992). Structural determinants of barium permeation and rectification in non-NMDA glutamate receptor channels. J. Neurosci. *12*, 4080–4087.

Durant, F., Bischof, J., Fields, C., Morokuma, J., Lapalme, J., Hoi, A., and Levin, M. (2019). The role of early bioelectric signals in the regeneration of planarian anterior/posterior polarity. Biophys. J. *116*, 948–961.

Durant, F., Morokuma, J., Fields, C., Williams, K., Adams, D.S., and Levin, M. (2017). Long-term, stochastic editing of regenerative anatomy via targeting endogenous bioelectric gradients. Biophys. J. *112*, 2231–2243.

Eaton, D.C., and Brodwick, M.S. (1980). Effects of barium on the potassium conductance of squid axon. J. Gen. Physiol. *75*, 727–750.

Elgart, M., Snir, O., and Soen, Y. (2015). Stress-mediated tuning of developmental robustness and plasticity in flies. Biochim. Biophys. Acta *1849*, 462–466.

Emmons-Bell, M., Durant, F., Hammelman, J., Bessonov, N., Volpert, V., Morokuma, J., Pinet, K., Adams, D.S., Pietak, A., Lobo, D., and Levin, M. (2015). Gap junctional blockade stochastically induces different species-specific head

anatomies in genetically wild-type *Girardia dorotocephala* flatworms. Int. J. Mol. Sci. *16*, 27865–27896.

Fern, R.F., Matute, C., and Stys, P.K. (2014). White matter injury: ischemic and nonischemic. Glia *62*, 1780–1789.

Freddolino, P.L., and Tavazoie, S. (2012). Beyond homeostasis: a predictive-dynamic framework for understanding cellular behavior. Annu. Rev. Cell Dev. Biol. *28*, 363–384.

Galinsky, R., Davidson, J.O., Lear, C.A., Bennet, L., Green, C.R., and Gunn, A.J. (2017). Connexin hemichannel blockade improves survival of striatal GABA-ergic neurons after global cerebral ischaemia in term-equivalent fetal sheep. Sci. Rep. *7*, 6304.

Gonzalez, A., and Bell, G. (2013). Evolutionary rescue and adaptation to abrupt environmental change depends upon the history of stress. Philos. Trans. R. Soc. Lond. B Biol. Sci. *368*, 20120079.

Greber, S., Schwarzer, C., and Sperk, G. (1994). Neuropeptide Y inhibits potassium-stimulated glutamate release through Y2 receptors in rat hippocampal slices in vitro. Br. J. Pharmacol. *113*, 737–740.

Grundemar, L., Wahlestedt, C., and Reis, D.J. (1991a). Long-lasting inhibition of the cardiovascular responses to glutamate and the baroreceptor reflex elicited by neuropeptide Y injected into the nucleus tractus solitarius of the rat. Neurosci. Lett. *122*, 135–139.

Grundemar, L., Wahlestedt, C., and Reis, D.J. (1991b). Neuropeptide Y acts at an atypical receptor to evoke cardiovascular depression and to inhibit glutamate responsiveness in the brainstem. J. Pharmacol. Exp. Ther. *258*, 633–638.

Hanrahan, J.W., Wills, N.K., Phillips, J.E., and Lewis, S.A. (1986). Basolateral K-channels in an insect epithelium - channel density, conductance, and block by barium. J. Gen. Physiol. *87*, 443–466.

Hasbani, M.J., Hyrc, K.L., Faddis, B.T., Romano, C., and Goldberg, M.P. (1998). Distinct roles for sodium, chloride, and calcium in excitotoxic dendritic injury and recovery. Exp. Neurol. *154*, 241–258.

Herrera-Rincon, C., Golding, A.S., Moran, K.M., Harrison, C., Martyniuk, C.J., Guay, J.A., Zaltsman, J., Carabello, H., Kaplan, D.L., and Levin, M. (2018). Brief local application of progesterone via a wearable bioreactor induces long-term regenerative response in adult *Xenopus* hindlimb. Cell Rep. *25*, 1593–1609.e7.

Hill, E.M., and Petersen, C.P. (2015). Wnt/Notum spatial feedback inhibition controls neoblast differentiation to regulate reversible growth of the planarian brain. Development *142*, 4217–4229.

Hockerman, G.H., Peterson, B.Z., Johnson, B.D., and Catterall, W.A. (1997). Molecular determinants of drug binding and action on L-type calcium channels. Annu. Rev. Pharmacol. Toxicol. *37*, 361–396.

Huang, S., Eichler, G., Bar-Yam, Y., and Ingber, D.E. (2005). Cell fates as high-dimensional attractor states of a complex gene regulatory network. Phys. Rev. Lett. *94*, 128701–212802.

Inoue, H., Ohtaki, H., Nakamachi, T., Shioda, S., and Okada, Y. (2007). Anion channel blockers attenuate delayed neuronal cell death induced by transient forebrain ischemia. J. Neurosci. Res. *85*, 1427–1435.

Inoue, T., Yamashita, T., and Agata, K. (2014). Thermosensory signaling by TRPM is processed by brain serotonergic neurons to produce planarian thermotaxis. J. Neurosci. *34*, 15701–15714.

Jiang, Y., and Mackinnon, R. (2000). The barium site in a potassium channel by x-ray crystallography. J. Gen. Physiol. *115*, 269–272.

Jollos, V. (1933). Further experimental tests on the problem of type deformation. Naturwissenschaften *21*, 455–456.

Jollos, V. (1934). Dauermodifikationen und mutationen bei protozoen. Arch. Protistenk *83*, 197–219.

Karin, O., Swisa, A., Glaser, B., Dor, Y., and Alon, U. (2016). Dynamical compensation in physiological circuits. Mol. Syst. Biol. *12*, 886.

Kim, E.Z., Vienne, J., Rosbash, M., and Griffith, L.C. (2017). Non-reciprocal homeostatic compensation in Drosophila potassium channel mutants. J. Neurophysiol. *117*, 2125–2136.

Kurachi, Y. (1986). Blocking effects of cesium and barium on the inward-rectifier K channel in the ventricular cell-membrane of the Guinea-pig. Jpn. Circ. J. *50*, 512.

Kussell, E., Kishony, R., Balaban, N.Q., and Leibler, S. (2005). Bacterial persistence: a model of survival in changing environments. Genetics *169*, 1807–1814.

Lai, T.W., Zhang, S., and Wang, Y.T. (2014). Excitotoxicity and stroke: identifying novel targets for neuroprotection. Prog. Neurobiol. *115*, 157–188.

Lambert, G., and Kussell, E. (2014). Memory and fitness optimization of bacteria under fluctuating environments. PLoS Genet. *10*, e1004556.

Lange, C.S., and Steele, V.E. (1978). The mechanism of anterior-posterior polarity control in planarians. Differentiation *11*, 1–12.

Lashinger, E.S., Steiginga, M.S., Hieble, J.P., Leon, L.A., Gardner, S.D., Nagilla, R., Davenport, E.A., Hoffman, B.E., Laping, N.J., and Su, X. (2008). AMTB, a TRPM8 channel blocker: evidence in rats for activity in overactive bladder and painful bladder syndrome. Am. J. Physiol. Renal Physiol., *295*, F803–F810.

Latorre, R., Hurst, R., Diaz, F., Toro, L., and Stefani, E. (1997). Barium as a probe of the molecular architecture of the pore of K+ channels. In From Ion Channels to Cell-To-Cell Conversations, R. Latorre and J. Saez, eds. (Plenum Press), pp. 129–146.

Lau, A., and Tymianski, M. (2010). Glutamate receptors, neurotoxicity and neurodegeneration. Pflugers Arch. *460*, 525–542.

Levin, M., Pietak, A.M., and Bischof, J. (2019). Planarian regeneration as a model of anatomical homeostasis: recent progress in biophysical and computational approaches. Semin. Cell Dev. Biol. *87*, 125–144.

Li, H., Huang, J., Du, W., Jia, C., Yao, H., and Wang, Y. (2012). TRPC6 inhibited NMDA receptor activities and protected neurons from ischemic excitotoxicity. J. Neurochem. *123*, 1010–1018.

Liang, D., Bhatta, S., Gerzanich, V., and Simard, J.M. (2007). Cytotoxic edema: mechanisms of pathological cell swelling. Neurosurg. Focus *22*, E2.

Liberante, F.G., Pouryahya, T., Mcmullin, M.F., Zhang, S.D., and Mills, K.I. (2016). Identification and validation of the dopamine agonist bromocriptine as a novel therapy for high-risk myelodysplastic syndromes and secondary acute myeloid leukemia. Oncotarget *7*, 6609–6619.

Lopez Garcia de Lomana, A., Kaur, A., Turkarslan, S., Beer, K.D., Mast, F.D., Smith, J.J., Aitchison, J.D., and Baliga, N.S. (2017). Adaptive prediction emerges over short evolutionary time scales. Genome Biol. Evol. *9*, 1616–1623.

Mark, L.P., Prost, R.W., Ulmer, J.L., Smith, M.M., Daniels, D.L., Strottmann, J.M., Brown, W.D., and Hacein-Bey, L. (2001). Pictorial review of glutamate excitotoxicity: fundamental concepts for neuroimaging. AJNR Am. J. Neuroradiol. *22*, 1813–1824.

Masotti, A., Uva, P., Davis-Keppen, L., Basel-Vanagaite, L., Cohen, L., Pisaneschi, E., Celluzzi, A., Bencivenga, P., Fang, M., Tian, M., et al. (2015). Keppen-lubinsky syndrome is caused by mutations in the inwardly rectifying K(+) channel encoded by KCNJ6. Am. J. Hum. Genet. *96*, 295–300.

Mccullough, L.A., Egan, T.M., and Westfall, T.C. (1998). Neuropeptide Y inhibition of calcium channels in PC-12 pheochromocytoma cells. Am. J. Physiol. *274*, C1290–C1297.

Mcmahon, H.T., and Nicholls, D.G. (1993). Barium-evoked glutamate release from Guinea-pig cerebrocortical synaptosomes. J. Neurochem. *61*, 110–115.

Mendonca-Silva, D.L., Novozhilova, E., Cobbett, P.J., Silva, C.L., Noel, F., Totten, M.I., Maule, A.G., and Day, T.A. (2006). Role of calcium influx through voltage-operated calcium channels and of calcium mobilization in the physiology of *Schistosoma mansoni* muscle contractions. Parasitology *133*, 67–74.

Ni, Y.L., Kuan, A.S., and Chen, T.Y. (2014). Activation and inhibition of TMEM16A calcium-activated chloride channels. PLoS One *9*, e86734.

Nogi, T., Zhang, D., Chan, J.D., and Marchant, J.S. (2009). A novel biological activity of praziquantel requiring voltage-operated Ca2+ channel beta subunits: subversion of flatworm regenerative polarity. PLoS Negl. Trop. Dis. *3*, e464.

Oda, T., Kume, T., Izumi, Y., Takada-Takatori, Y., Niidome, T., and Akaike, A. (2008). Bromocriptine, a dopamine D(2) receptor agonist with the structure of the amino acid ergot alkaloids, induces neurite outgrowth in PC12 cells. Eur. J. Pharmacol. *598*, 27–31.

Odaka, H., Numakawa, T., Adachi, N., Ooshima, Y., Nakajima, S., Katanuma, Y., Inoue, T., and Kunugi, H. (2014). Cabergoline, dopamine D2 receptor agonist, prevents neuronal cell death under oxidative stress via reducing excitotoxicity. PLoS One *9*, e99271.

Oviedo, N.J., Morokuma, J., Walentek, P., Kema, I.P., Gu, M.B., Ahn, J.M., Hwang, J.S., Gojobori, T., and Levin, M. (2010). Long-range neural and gap junction protein-mediated cues control polarity during planarian regeneration. Dev. Biol. *339*, 188–199.

Oviedo, N.J., Nicolas, C.L., Adams, D.S., and Levin, M. (2008). Live imaging of planarian membrane potential using DiBAC4(3). Cold Spring Harb. Protoc. *2008*, pdb.prot5055.

Owlarn, S., and Bartscherer, K. (2016). Go ahead, grow a head! A planarian's guide to anterior regeneration. Regeneration (Oxf.) *3*, 139–155.

Pai, V.P., Pietak, A., Willocq, V., Ye, B., Shi, N.Q., and Levin, M. (2018). HCN2 Rescues brain defects by enforcing endogenous voltage pre-patterns. Nat. Commun. *9*, 998.

Pardo, L.A., and Stuhmer, W. (2014). The roles of K(+) channels in cancer. Nat. Rev. Cancer *14*, 39–48.

Parmar, N.S., Tariq, M., and Ageel, A.M. (1984). Effect of bromocriptine, a dopamine receptor agonist, on the experimentally induced gastric ulcers in albino rats. Life Sci. *35*, 2035–2039.

Pellettieri, J., and Sánchez Alvarado, A. (2007). Cell turnover and adult tissue homeostasis: from humans to planarians. Annu. Rev. Genet. *41*, 83–105.

Petralia, R.S., Mattson, M.P., and Yao, P.J. (2014). Aging and longevity in the simplest animals and the quest for immortality. Ageing Res. Rev. *16*, 66–82.

Pezzulo, G., and Levin, M. (2015). Re-membering the body: applications of computational neuroscience to the top-down control of regeneration of limbs and other complex organs. Integr. Biol. (Camb.) *7*, 1487–1517.

Pietak, A., and Levin, M. (2016). Exploring instructive physiological signaling with the bioelectric tissue simulation engine. Front. Bioeng. Biotechnol. *4*, 55.

Prentice, H., Modi, J.P., and Wu, J.Y. (2015). Mechanisms of neuronal protection against excitotoxicity, endoplasmic reticulum stress, and mitochondrial dysfunction in stroke and neurodegenerative diseases. Oxid. Med. Cell Longev. *2015*, 964518.

Prymaczok, N.C., Pasqualino, V.M., Viau, V.E., Rodriguez, E.M., and Medesani, D.A. (2016). Involvement of the crustacean hyperglycemic hormone (CHH) in the physiological compensation of the freshwater crayfish *Cherax quadricarinatus* to low temperature and high salinity stress. J. Comp. Physiol. B *186*, 181–191.

Quayle, J.M., Standen, N.B., and Stanfield, P.R. (1988). The voltage-dependent block of ATP-sensitive potassium channels of frog skeletal muscle by caesium and barium ions. J. Physiol. *405*, 677–697.

Reddien, P.W. (2018). The cellular and molecular basis for planarian regeneration. Cell *175*, 327–345.

Rubin, H. (1985). Cancer as a dynamic developmental disorder. Cancer Res. *45*, 2935–2942.

Rubin, H. (2006). What keeps cells in tissues behaving normally in the face of myriad mutations? BioEssays *28*, 515–524.

Rubin, H. (2007). Ordered heterogeneity and its decline in cancer and aging. Adv. Cancer Res. *98*, 117–147.

Rungta, R.L., Choi, H.B., Tyson, J.R., Malik, A., Dissing-Olesen, L., Lin, P.J.C., Cain, S.M., Cullis, P.R., Snutch, T.P., and Macvicar, B.A. (2015). The cellular mechanisms of neuronal swelling underlying cytotoxic edema. Cell *161*, 610–621.

Sahu, S., Dattani, A., and Aboobaker, A.A. (2017). Secrets from immortal worms: what can we learn about biological ageing from the planarian model system? Semin. Cell Dev. Biol. *70*, 108–121.

Saló, E., Abril, J.F., Adell, T., Cebrià, F., Eckelt, K., Fernandez-Taboada, E., Handberg-Thorsager, M., Iglesias, M., Molina, M.D., and Rodríguez-Esteban, G. (2009). Planarian regeneration: achievements and future directions after 20 years of research. Int. J. Dev. Biol. *53*, 1317–1327.

Samani, P., and Bell, G. (2016). The ghosts of selection past reduces the probability of plastic rescue but increases the likelihood of evolutionary rescue to novel stressors in experimental populations of wild yeast. Ecol. Lett. *19*, 289–298.

Sarnat, H.B., and Netsky, M.G. (1985). The brain of the planarian as the ancestor of the human brain. Can. J. Neurol. Sci. *12*, 296–302.

Schneider, M.B., Murrin, L.C., Pfeiffer, R.F., and Deupree, J.D. (1984). Dopamine receptors: effects of chronic L-dopa and bromocriptine treatment in an animal model of Parkinson's disease. Clin. Neuropharmacol. *7*, 247–257.

Schriever, A.M., Friedrich, T., Pusch, M., and Jentsch, T.J. (1999). CLC chloride channels in *Caenorhabditis elegans*. J. Biol. Chem. *274*, 34238–34244.

Sihra, T.S., Piomelli, D., and Nichols, R.A. (1993). Barium evokes glutamate release from rat brain synaptosomes by membrane depolarization: involvement of K+, Na+, and Ca2+ channels. J. Neurochem. *61*, 1220–1230.

Silva, A.P., Xapelli, S., Pinheiro, P.S., Ferreira, R., Lourenço, J., Cristóvão, A., Grouzmann, E., Cavadas, C., Oliveira, C.R., and Malva, J.O. (2005). Up-regulation of neuropeptide Y levels and modulation of glutamate release through neuropeptide Y receptors in the hippocampus of kainate-induced epileptic rats. J. Neurochem. *93*, 163–170.

Simons, C., Rash, L.D., Crawford, J., Ma, L., Cristofori-Armstrong, B., Miller, D., Ru, K., Baillie, G.J., Alanay, Y., Jacquinet, A., et al. (2015). Mutations in the voltage-gated potassium channel gene KCNH1 cause Temple-Baraitser syndrome and epilepsy. Nat. Genet. *47*, 73–77.

Skaper, S.D. (2011). Ion channels on microglia: therapeutic targets for neuroprotection. CNS Neurol. Disord. Drug Targets *10*, 44–56.

Soen, Y., and Braun, E. (2000). Scale-invariant fluctuations at different levels of organization in developing heart cell networks. Phys. Rev. E Stat. Phys. Plasmas Fluids Relat. Interdiscip. Top. *61*, R2216–R2219.

Soen, Y., Knafo, M., and Elgart, M. (2015). A principle of organization which facilitates broad Lamarckian-like adaptations by improvisation. Biol. Direct *10*, 68.

Sorek, M., Balaban, N.Q., and Loewenstein, Y. (2013). Stochasticity, bistability and the wisdom of crowds: a model for associative learning in genetic regulatory networks. PLoS Comput. Biol. *9*, e1003179.

Stern, S., Fridmann-Sirkis, Y., Braun, E., and Soen, Y. (2012). Epigenetically heritable alteration of fly development in response to toxic challenge. Cell Rep. *1*, 528–542.

Stetina, T., Kostal, V., and Korbelova, J. (2015). The role of inducible Hsp70, and other heat shock proteins, in adaptive complex of cold tolerance of the fruit fly (*Drosophila melanogaster*). PLoS One *10*, e0128976.

Sullivan, K.G., Emmons-Bell, M., and Levin, M. (2016). Physiological inputs regulate species-specific anatomy during embryogenesis and regeneration. Commun. Integr. Biol. *9*, e1192733.

Szydlowska, K., and Tymianski, M. (2010). Calcium, ischemia and excitotoxicity. Cell Calcium *47*, 122–129.

Takeuchi, H., Mizoguchi, H., Doi, Y., Jin, S., Noda, M., Liang, J., Li, H., Zhou, Y., Mori, R., Yasuoka, S., et al. (2011). Blockade of gap junction hemichannel suppresses disease progression in mouse models of amyotrophic lateral sclerosis and Alzheimer's disease. PLoS One *6*, e21108.

Tanaka, E.M., and Reddien, P.W. (2011). The cellular basis for animal regeneration. Dev. Cell *21*, 172–185.

Tarkowski, A.K. (1961). Mouse chimaeras developed from fused eggs. Nature *190*, 857–860.

Thompson, R.J. (2015). Pannexin channels and ischaemia. J. Physiol. *593*, 3463–3470.

Tkachenko, A.G. (2018). Stress responses of bacterial cells as mechanism of development of antibiotic tolerance (review). Appl. Biochem. Microbiol. *54*, 108–127.

Urrego, D., Tomczak, A.P., Zahed, F., Stuhmer, W., and Pardo, L.A. (2014). Potassium channels in cell cycle and cell proliferation. Philos. Trans. R Soc. Lond. B Biol. Sci. *369*, 20130094.

Vaarmann, A., Kovac, S., Holmstrom, K.M., Gandhi, S., and Abramov, A.Y. (2013). Dopamine protects neurons against glutamate-induced excitotoxicity. Cell Death Dis. *4*, e455.

Vandenberg, L.N., Adams, D.S., and Levin, M. (2012). Normalized shape and location of perturbed craniofacial structures in the *Xenopus* tadpole reveal an innate ability to achieve correct morphology. Dev. Dyn. *241*, 863–878.

Via, M.A., Chandra, H., Araki, T., Potenza, M.V., and Skamagas, M. (2010). Bromocriptine approved as the first medication to target dopamine activity to improve glycemic control in patients with type 2 diabetes. Diabetes Metab. Syndr. Obes. *3*, 43–48.

Walter, S.J., Shirley, D.G., Folkerd, E.J., and Unwin, R.J. (2001). Effects of the Potassium channel blocker barium on sodium and potassium transport in the rat loop of Henle in vivo. Exp. Physiol. *86*, 469–474.

Wang, Y., Denisova, J.V., Kang, K.S., Fontes, J.D., Zhu, B.T., and Belousov, A.B. (2010). Neuronal gap junctions are required for NMDA receptor-mediated excitotoxicity: implications in ischemic stroke. J. Neurophysiol. *104*, 3551–3556.

Wang, Y., Song, J.H., Denisova, J.V., Park, W.M., Fontes, J.D., and Belousov, A.B. (2012). Neuronal gap junction coupling is regulated by glutamate and plays critical role in cell death during neuronal injury. J. Neurosci. *32*, 713–725.

White, M.M., and Aylwin, M. (1990). Niflumic and flufenamic acids are potent reversible blockers of Ca2(+)-activated Cl- channels in Xenopus oocytes. Mol. Pharmacol. *37*, 720–724.

Whittaker, E., Vereker, E., and Lynch, M.A. (1999). Neuropeptide Y inhibits glutamate release and long-term potentiation in rat dentate gyrus. Brain Res. *827*, 229–233.

Wright, S.H. (2004). Generation of resting membrane potential. Adv. Physiol. Educ. *28*, 139–142.

Wu, G., and Hamill, O.P. (1992). NPPB block of Ca(++)-activated Cl- currents in Xenopus oocytes. Pflugers Arch. *420*, 227–229.

Yapa, K., Deuis, J., Peters, A.A., Kenny, P.A., Roberts-Thomson, S.J., Vetter, I., and Monteith, G.R. (2018). Assessment of the TRPM8 inhibitor AMTB in breast cancer cells and its identification as an inhibitor of voltage gated sodium channels. Life Sci. *198*, 128–135.

Yokobori, S., Mazzeo, A.T., Hosein, K., Gajavelli, S., Dietrich, W.D., and Bullock, M.R. (2013). Preconditioning for traumatic brain injury. Transl Stroke Res. *4*, 25–39.

Zhang, Y., and Bhavnani, B.R. (2005). Glutamate-induced apoptosis in primary cortical neurons is inhibited by equine estrogens via down-regulation of caspase-3 and prevention of mitochondrial cytochrome c release. BMC Neurosci. *6*, 13.

Zheng, F., and Phelan, K.D. (2014). The role of canonical transient receptor potential channels in seizure and excitotoxicity. Cells *3*, 288–303.

Zhou, Y., Zeng, X.H., and Lingle, C.J. (2012). Barium ions selectively activate BK channels via the Ca2+-bowl site. Proc. Natl. Acad. Sci. U S A *109*, 11413–11418.

ISCI, Volume *22*

Supplemental Information

Regenerative Adaptation to Electrochemical Perturbation in Planaria: A Molecular Analysis of Physiological Plasticity

Maya Emmons-Bell, Fallon Durant, Angela Tung, Alexis Pietak, Kelsie Miller, Anna Kane, Christopher J. Martyniuk, Devon Davidian, Junji Morokuma, and Michael Levin

Supplemental Information

Supplemental Figures

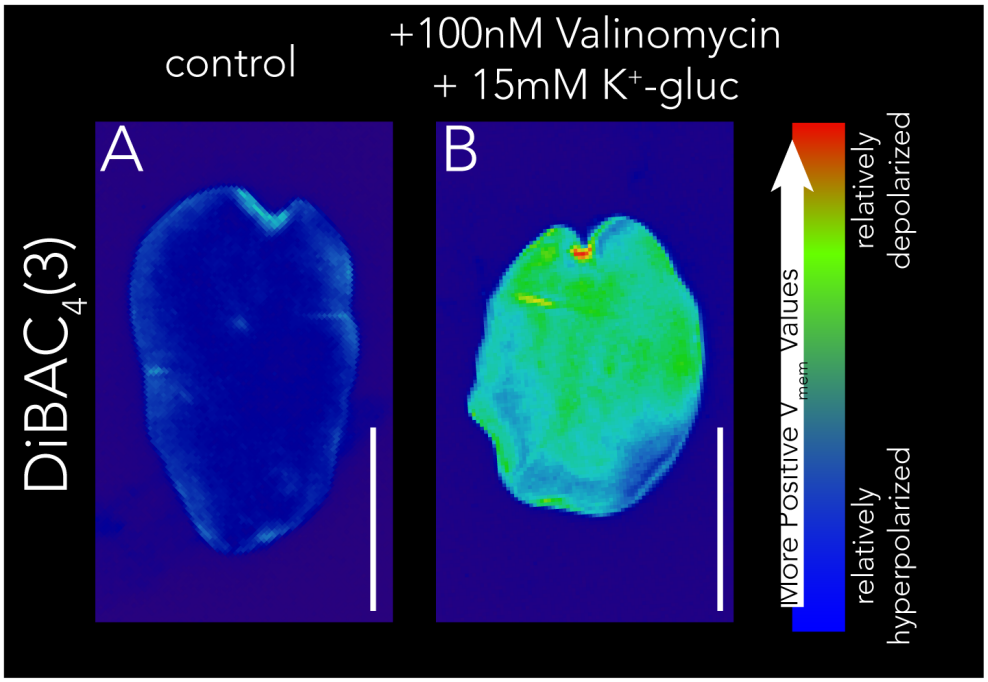

Figure S1. Valinomycin and potassium gluconate-induced depolarization can be visualized with $DiBAC_4(3)$, Related to Figure 3. Pretail fragments (fragments that contain the trunk region of the worm posterior to the pharynx and anterior to the tail) of *Dugesia japonica* were cut and placed into vehicle (**A**) or 100nM Valinomycin + 15mM potassium gluconate (K^+-gluc) (**B**) for 1 hour, then mounted and imaged. Both Valinomycin and K^+-gluc were used to optimize depolarization. Images were taken of ventral surface of fragment and were far-field and dark-field corrected. Images are pseudocolored to allow for ease of visualization of depolarization patterns, but worms were imaged in the same frame so as not to confound data after pseudocoloring, and all image analysis was done using raw images. Scale bars 0.5mm.

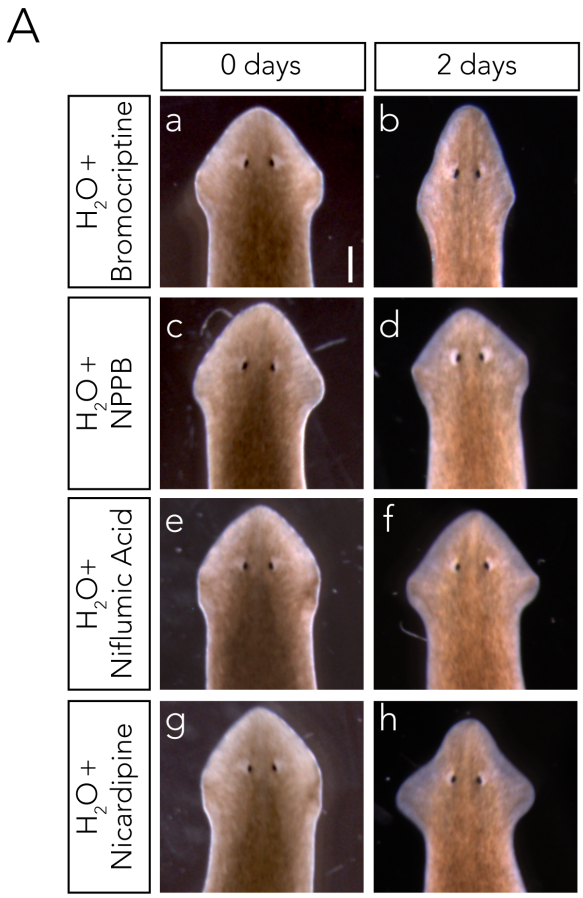

Figure S2. Drug treatment alone does not affect planaria, Related to Figure 4. (**A**) Exposure to Bromocriptine (**a**,**b**), NPPB (**c**,**d**), Niflumic acid (**e**,**f)**, or Nicardipine (**g**,**h**) for 2 days had no observable effect on *D. japonica* morphology.

Supplemental Tables

Table S2. Data statistics for RNA-seq, Related to Figure 2 and Tables 1 and 3. The 40 bp single end reads generated by Illumina HiSeq 2500 were quality checked and processed to remove the low quality bases and the adapter contamination. The table below lists the data generated for the individual samples.

Sample name	Chemistry	Barcode sequences	Total number of reads generated Post-processing (in millions)
WildType Head 2	40*1	TS13-AGTCAA	33.67
WildType Head 1	40*1	TS12-CTTGTA	39.18
BaCl2 Head 2	40*1	TS11-GGCTAC	36.72
BaCl2 Head 1	40*1	TS10-TAGCTT	34.64

Table S3. Alignment statistics for RNA-seq experiments, Related to Figure 2 and Tables 1 and 3. As the gene feature file for *Dugesia japonica* is not available, the reads were aligned to the *Dugesia japonica* (complete CDS regions) taken from NCBI (https://www.ncbi.nlm.nih.gov/nuccore/? term=Dugesia%20japonica) which consists of 138,026 nucleotide sequences, downloaded from the NCBI database using Tophat. The table below shows the alignment percentage of the reads mapped to the reference.

Sample name	No of reads (in millions)	Alignment percentage
WildType Head 2	33.67	92.60%
WildType Head 1	39.18	94.30%
BaCl2 Head 2	36.72	93.90%
BaCl2 Head 1	34.64	96.20%

Table S4. Gene Ontology Analysis, Related to Figure 2 and Tables 1 and 3. Most significant gene ontology categories affected at the transcript level with $BaCl_2$. All data for gene ontology can be found in Table S5.

Go Term Theme	***Category***	***Frequency***	***PAGE Z-Score***	***PAGE Raw p-value***	***FDR***
Biological Process	translation [go:0006412]	96	6.602042	4.06E-11	5.72E-09
	intracellular protein transport [go:0006886]	53	2.867622	0.004136	0.291566
	cell cycle [go:0007049]	17	-2.63838	0.00833	0.391526
	tricarboxylic acid cycle [go:0006099]	21	2.35727	0.01841	0.439486
	transmembrane receptor protein tyrosine kinase signaling pathway	5	2.270731	0.023163	0.439486
	pyrimidine nucleotide biosynthetic process [go:0006221]	5	2.248818	0.024524	0.439486
	protein glycosylation [go:0006486]	29	2.239905	0.025097	0.439486
	dna recombination [go:0006310]	8	-2.21806	0.026551	0.439486
	de novo' pyrimidine nucleobase biosynthetic process [go:0006207]	6	2.196554	0.028052	0.439486
	dna integration [go:0015074]	20	-2.14806	0.031709	0.447092
	malate metabolic process [go:0006108]	6	-2.03848	0.041502	0.492306
	vesicle-mediated transport [go:0016192]	35	1.986827	0.046942	0.492306
Molecular Function	structural constituent of cytoskeleton [go:0005200]	89	-7.40681	1.29E-13	2.69E-11
	structural constituent of ribosome [go:0003735]	100	6.812948	9.56E-12	9.94E-10
	acyl-coa dehydrogenase activity [go:0003995]	9	3.133764	0.001726	0.119655
	nad-dependent histone deacetylase activity (h3-k14 specific)	7	3.026156	0.002477	0.128796
	nad+ kinase activity [go:0003951]	7	2.825761	0.004717	0.196221

	proton-transporting atp synthase activity, rotational mechanism	7	2.604398	0.009204	0.275972
	protein tyrosine phosphatase activity [go:0004725]	38	-2.54166	0.011033	0.275972
	nucleotidyltransferase activity [go:0016779]	12	2.513792	0.011944	0.275972
	microtubule binding [go:0008017]	39	-2.45754	0.013989	0.275972
	mannosyl-oligosaccharide 1,2-alpha-mannosidase activity	8	2.449566	0.014303	0.275972
	extracellular matrix structural constituent [go:0005201]	16	-2.43919	0.01472	0.275972
	flavin adenine dinucleotide binding [go:0050660]	27	2.410711	0.015921	0.275972
	histone-lysine n-methyltransferase activity [go:0018024]	14	2.330139	0.019799	0.297096
	inorganic anion exchanger activity [go:0005452]	7	2.326406	0.019997	0.297096
	carboxypeptidase activity [go:0004180]	7	2.091671	0.036468	0.425427
	peptidyl-dipeptidase activity [go:0008241]	7	2.091671	0.036468	0.425427
	chromatin binding [go:0003682]	9	2.068059	0.038634	0.425427
	ubiquitin-protein transferase activity [go:0004842]	48	2.020134	0.043369	0.425427
	phospholipid binding [go:0005543]	6	1.997395	0.045782	0.425427
	carbohydrate binding [go:0030246]	16	1.970462	0.048785	0.425427
Cellular Component	ribosome [go:0005840]	83	5.158659	2.49E-07	1.77E-05
	small ribosomal subunit [go:0015935]	9	3.061898	0.002199	0.078078
	cytosol [go:0005829]	11	2.920361	0.003496	0.082745
	nucleolus [go:0005730]	21	-2.30831	0.020982	0.346204
	large ribosomal subunit [go:0015934]	10	2.206271	0.027365	0.346204

	extracellular space [go:0005615]	15	2.180011	0.029257	0.346204
	motile cilium [go:0031514]	7	-2.04248	0.041104	0.416915

Table S6. Lists of genes depicted in Figure 2A and B, Related to Figure 2. (**A**) Full list of altered anion transport-related genes shown in Figure 2A. (**B**) Full list of altered transmission of nerve impulse-related genes shown in Figure 2C.

Table 6A

Name	***Probe Value***	***Description***
ABCA1	1.0018	ATP-binding cassette, sub-family A (ABC1), member 1
SLC12A2	0.3578	solute carrier family 12 (sodium/potassium/chloride transporters), member 2
SLC26A3	-2.0998	solute carrier family 26 (anion exchanger), member 3
SLC4A3	0.0388	solute carrier family 4, anion exchanger, member 3
SLC26A4	-1.201	solute carrier family 26, member 4
SLC17A1	10.9346	solute carrier family 17 (organic anion transporter), member 1
SLC22A11	3.5889	solute carrier family 22 (organic anion/urate transporter), member 11
ABCC3	1.3558	ATP-binding cassette, sub-family C (CFTR/MRP), member 3
SLCO1A2	-1.2222	solute carrier organic anion transporter family, member 1A2
ABCC2	-0.4388	ATP-binding cassette, sub-family C (CFTR/MRP), member 2
ABCC1	-0.896	ATP-binding cassette, sub-family C (CFTR/MRP), member 1
SLC22A6	-1.1533	solute carrier family 22 (organic anion transporter), member 6
ABCB1	-0.896	ATP-binding cassette, sub-family B (MDR/TAP), member 1
CAT	0.4148	catalase
UCP1	-0.2243	uncoupling protein 1 (mitochondrial, proton carrier)
TSPO	0.6788	translocator protein (18kDa)
m_Slco1a1	-1.2222	solute carrier organic anion transporter family, member 1a1

Table 6B

Name	**Probe Value**	**Description**
CTNNB1	-3.0765	catenin (cadherin-associated protein), beta 1, 88kDa
SLC8A1	1.8271	solute carrier family 8 (sodium/calcium exchanger), member 1

SLC12A2	0.3578	solute carrier family 12 (sodium/potassium/chloride transporters), member 2
SLC4A3	0.0388	solute carrier family 4, anion exchanger, member 3
GRIA2	0.3083	glutamate receptor, ionotropic, AMPA 2
GRIK2	2.546	glutamate receptor, ionotropic, kainate 2
TRPC3	0.5344	transient receptor potential cation channel, subfamily C, member 3
ASIC5	2.4432	acid-sensing (proton-gated) ion channel family member 5
P2RX4	0.8279	purinergic receptor P2X, ligand-gated ion channel, 4
CACNA2D1	1.3416	calcium channel, voltage-dependent, alpha 2/delta subunit 1
KCNA3	0.8759	potassium voltage-gated channel, shaker-related subfamily, member 3
KCNC2	-1.0571	potassium voltage-gated channel, Shaw-related subfamily, member 2
KCNH2	0.7843	potassium voltage-gated channel, subfamily H (eag-related), member 2
CAT	0.4148	catalase
FAAH	-0.8367	fatty acid amide hydrolase
GLUL	-1.415	glutamate-ammonia ligase
NPR1	0.6392	natriuretic peptide receptor A/guanylate cyclase A (atrionatriuretic peptide receptor A)
DAO	1.1035	D-amino-acid oxidase
ERG	1.5128	v-ets erythroblastosis virus E26 oncogene homolog (avian)
FOS	-0.2607	FBJ murine osteosarcoma viral oncogene homolog
JUN	0.3939	jun proto-oncogene
REST	-0.1284	RE1-silencing transcription factor
EGFR	1.2985	epidermal growth factor receptor
MEN1	-1.3847	multiple endocrine neoplasia I
MARK2	-1.9312	MAP/microtubule affinity-regulating kinase 2
UBC	0.2766	ubiquitin C
RANBP2	-0.375	RAN binding protein 2
CAV1	-1.0436	caveolin 1, caveolae protein, 22kDa
SNAP25	-0.228	synaptosomal-associated protein, 25kDa
ANK2	1.1996	ankyrin 2, neuronal
KIF5B	-0.1274	kinesin family member 5B
PANX1	-3.5446	pannexin 1
AGRN	-1.2874	agrin
GFAP	1.8981	glial fibrillary acidic protein
NALCN	0.8476	sodium leak channel, non-selective
INS	1.5798	insulin
NTN1	1.616	netrin 1
TNF	-0.25	tumor necrosis factor
CDC42	-0.2927	cell division cycle 42 (GTP binding protein)
RAC1	0.0752	ras-related C3 botulinum toxin substrate 1 (rho family, small GTP binding protein Rac1)

RAP1B	0.6267	RAP1B, member of RAS oncogene family
RASGRF1	-0.9149	Ras protein-specific guanine nucleotide-releasing factor 1
MYLK	1.7125	myosin light chain kinase
CASP3	-0.7907	caspase 3, apoptosis-related cysteine peptidase
GPER1	0.3777	G protein-coupled estrogen receptor 1
NPY1R	85.4924	neuropeptide Y receptor Y1
CXCR4	85.4924	chemokine (C-X-C motif) receptor 4
MMP9	3.4586	matrix metallopeptidase 9 (gelatinase B, 92kDa gelatinase, 92kDa type IV collagenase)
CDK5	-0.2833	cyclin-dependent kinase 5
BRSK2	-0.8513	BR serine/threonine kinase 2
RAB8A	2.13	RAB8A, member RAS oncogene family
RAB10	0.0681	RAB10, member RAS oncogene family
APC	1.0329	adenomatous polyposis coli
PICK1	1.3926	protein interacting with PRKCA 1
ACE	0.9108	angiotensin I converting enzyme (peptidyl-dipeptidase A) 1
PRMT1	-0.1001	protein arginine methyltransferase 1
DBI	-0.085	diazepam binding inhibitor (GABA receptor modulator, acyl-Coenzyme A binding protein)
TSPO	0.6788	translocator protein (18kDa)
MSRA	-1.1203	methionine sulfoxide reductase A
PITPNA	-0.3698	phosphatidylinositol transfer protein, alpha
GRIK1	-3.1039	glutamate receptor, ionotropic, kainate 1

Transparent Methods

Planarian care

A clonal strain of *Dugesia japonica* was maintained at 13 °C in Poland Spring water with weekly feedings of liver paste and twice-weekly water changes, as in (Oviedo et al., 2008a). Worms were maintained at 13°C for the duration of the experiment in order to prevent spontaneous fissioning, which occurs at a greater rate at higher temperatures and which would interfere with interpretation of results regarding timing of regeneration (Oviedo et al., 2008a). Due to experimental temperature being 13°C, worms were taken from a cold-adapted 13 °C colony which is continuously maintained at that temperature. Worms were starved for at least one week prior to the beginning of each experiment.

$BaCl_2$ Adaptation and Loss of Adaptation

Whole worms were maintained at 13 °C in untreated tissue culture plates containing either Poland Spring water or 1 mM $BaCl_2$ (MP Biomedicals Inc) in Poland Spring water ($BaCl_2$ solution). Both water and $BaCl_2$ solutions were replaced once a week. A maximum of 30 worms were kept in each plate (diameter 100 mm), which contained approximately 50 mL of solution. Progression of response to $BaCl_2$ was assessed by regular examination of animals using a stereoscope. Worms that had fully regenerated in refreshed $BaCl_2$ for at least three weeks and were indistinguishable in appearance from untreated worms were designated "$BaCl_2$-adapted worms."

To assess the persistence of the $BaCl_2$ adaptation, $BaCl_2$-adapted worms were removed from the 1mM $BaCl_2$ solution and maintained in untreated tissue culture plates at 13 °C in Poland Spring water for 30 days before being placed again in 1mM $BaCl_2$ solution.

Drug treatments: $BaCl_2$ and ion channel blockers

In order to test the effects of particular channels on $BaCl_2$ adaptation, planaria were exposed to 1mM $BaCl_2$ in the presence of drugs that modify channels. In each case, planaria were exposed to either $BaCl_2$+treatment solution (Poland Spring water with 1 mM $BaCl_2$ and the respective drug) as well as 3 control solutions. Control solutions were Poland Spring water plus matching concentration of DMSO, drug control solution (Poland Spring water plus the drug (dissolved in DMSO)), or BaCl2-control solution (Poland Spring water, 1mM BaCl, and matching DMSO concentration). DMSO concentration never exceeded .1% as higher concentrations have been shown to interfere with normal planarian function (Pagan et al., 2006, Stevens et al., 2015, Yuan et al., 2012). Worms were maintained in tissue culture treated dishes at 13 °C. Multiple concentrations were tested for each drug, and the lowest effective concentration was used for each.

Bromocriptine mesylate at a final concentration of 0.5 μM (Tocris #0427), dissolved in Poland Spring from a stock dissolved in DMSO (final DMSO concentration: 0.0075%) was used to block monoamines. Inhibition of calcium activated chloride channels was performed using 5.0 μM 5-Nitro-2-(3-phenylpropylamino)benzoic acid (NPPB, Cayman Chemical #17292) or 1.25 μM niflumic acid (Tocris #4112) in Poland Spring from a stock dissolved in DMSO (final DMSO concentration 0.006% or 0.000726%, respectively). Inhibition of calcium channels was performed using 2.5 μM nicardipine hydrochloride (Sigma-Aldrich #N7510) in Poland Spring from a stock dissolved in DMSO (final concentration of DMSO 0.0025%). Inhibition of TRPM was achieved using 100 μM AMTB hydrochloride (Tocris #3989) in Poland Spring from a stock dissolved in DMSO (final concentration of DMSO 0.1%). For AMTB treatments, media was refreshed once a week, all other solutions were refreshed every two days.

Visualization of relative membrane potentials with $DiBAC_4(3)$ dye imaging

$DiBAC_4(3)$ (bis-(1,3-dibutylbarbituric acid)-trimethine oxanol) (Invitrogen) was used as previously described (Oviedo et al., 2008b). Briefly, a stock solution (1.9 mM) was diluted 1:1000 (1.9 µM) in Poland Spring water or 1 mM $BaCl_2$ solution, and worms were soaked in the $DiBAC_4(3)$ solution for >30 minutes before imaging. Worms were then immobilized in 2% low-meting point agarose, using custom-fabricated Planarian Immobilization Chips as per Dexter and colleagues (Dexter et al., 2014). Images of the ventral side of immobilized planaria were captured with the Nikon AZ100 Stereomicroscope using epifluorescence optics and NIS-Elements imaging software. Treatment and control animals were captured within the same frame and care was taken to ensure that planaria did not move during image acquisition. No data points or image features were removed from our analysis. To quantify differences in relative depolarization, average pixel intensity of the head region, defined as the anterior $1/6^{th}$ of the worm, was quantified with ImageJ, after flat-field correction. This treatment avoided confounding the analysis by including fluorescence due to background and slime.

RNA extraction and RNA-seq

Total RNA was extracted from wild type and $BaCl_2$-adapted *D. japonica* heads. Two biological replicates were collected for each treatment, with 25 worms pooled per replicate. Worms were kept in 1 mM $BaCl_2$ for 35 days, when $BaCl_2$-insensitive heads had fully regenerated. Heads (as defined by the anterior $1/6^{th}$ of the worm) were then amputated and RNA was extracted using Trizol (Ambion/ThermoFisher) as per the manufacturer's instructions. RNA was pelleted via isopropanol extraction and then suspended in 80% ethanol. Following DNase-treatment, the concentration of RNA was crudely quantified via NanoDrop™, and samples were stored at -80°C. Samples were sent to the Whitehead Institute Genome Technology Core for sequencing. Quality control for RNA was conducted using an Agilent 2100 Bioanalyzer. While RIN scores cannot be used with planarian species due to an absence of 28s rRNA peaks (Kim, 2019, Liu and Rink, 2018), we confirmed quality of RNA prior to library prep with the sequencing core. Library prep was performed on high quality RNA using the TruSeq PolyA kit (Illumina) as per manufacturer's protocol. All sequencing libraries were then quantified, pooled and sequenced at single-end 40 base-pair using the Illumina HiSeq 2500. Following sequencing, data processing was done using the standard Illumina pipeline and Fastq files were generated for data processing and assembly.

Data Processing and Assembly

Raw Illumina files were processed by Genotypic Technology Ltd. (Bangalore, India) for read mapping and the identification of differentially expressed transcripts. Raw data were downloaded and processed (Adapter, B-block and low-quality base filtering) using Genotypic's proprietary Perl script for removing adapter and low-quality base trimming. RNA-Seq reads were then mapped using the ultra-high-throughput short read aligner Bowtie (Langmead, 2010) and reference alignment was conducted with TopHat-2.0.13 (Trapnell et al., 2009), a fast splice junction mapper for RNA-Seq reads. Processed data were inputted into TopHat and default parameters for directional libraries were used. Cufflinks-2.2.1 was used to assemble transcripts and to identify transcripts that were differentially expressed using default settings and -G option to facilitate read mapping. Biological replicates were combined using Cuffmerge and then analyzed using CuffDiff (2.2.1) for replicate samples by modeling the variance in fragment counts across replicates as a function of the mean fragment count. Each replicated condition was first used to build a model. Models were generated from each biological replicate and were averaged to provide a single global model for all conditions in the experiment. Cuffdiff was then used

to determine significant changes in transcript levels. Data and alignment statistics for the Illumina runs are presented in Tables S2 and S3.

Expression level estimation was reported as fragments per kilobase of transcript sequence per million mapped fragments (FPKM) value together with confidence intervals. The false discovery rate or FDR-adjusted p-value of the test statistic (q-value) was also generated. An in-house pipeline was developed to automate the abovementioned mapping and assembly process. All transcripts were annotated for Gene Ontology (GO) by performing a blast alignment. The 138,026 transcript sequences of *D. japonica* were subjected to blast against the 385,255 sequences of Platyhelminthes database extracted from Uniprot as a reference. Table S1 contains all processed transcript data, including fold change and p-value.

Pathway Studio 10.0 (Elsevier) and ResNet 11.0 were used for sub-network enrichment analysis (SNEA) of cell processes. The option of "best p value, highest magnitude fold change" in Pathway Studio was used for duplicated probes. Transcripts were successfully mapped using Name and Alias. SNEA was performed to identify gene networks that were significantly different in the treatment samples compared to control. A Kolmogorov–Smirnov test with 1000 permutations was conducted to determine whether specific networks were preferentially regulated compared to the background reference probability distribution. Networks were constructed based on common regulators of expression and regulators of specific cell processes. The enrichment p-value for a gene seed was set at $p< 0.05$. Additional details on the use of SNEA can be found in (Langlois and Martyniuk, 2013).

qPCR

1 µg total RNA extracted from the anterior 1/6th of *Dugesia japonica* was DNase treated and used as a template to synthesize cDNA (iScript gDNA Clear cDNA Synthesis Kit, BioRad, USA). PCR primers for Dj-TRPMa were obtained from the Agata lab (Inoue et al., 2014). Slc2a1 primers (F: 5'-TTGAACGATTCCGACCGCA-3', R: 5'-GGGTTTGCTTTGGGACTAGGA-3') were designed based on the upregulated sequences identified in the RNAseq analysis and were validated using melt curve analysis. GAPDH (Takano et al., 2007) was used as the reference gene. For qPCR, each 10 µL reaction was run in duplicate and contained: 5 µL of 2x PowerUp SYBR Green Master Mix (Applied Biosystems, USA), 0.5 µL of 10 µM of forward and reverse gene-specific primers, and 1.33 µL of diluted (1:20 for Slc2a1, 1:5 for Dj-TRPMa) cDNA template. qPCR was performed using the Step One Plus Real Time System (Applied Biosystems, USA) according to manufacturer's instructions. Relative expression was analyzed using the Pfaffl method (Pfaffl, 2001).

Data and Software Availability

RNA-Seq unprocessed data has been deposited in the National Center for Biotechnology Information (NCBI) Gene Expression Omnibus (GEO) and is accessible through GEO Series accession number (GSE98084).

Supplemental References

DEXTER, J. P., TAMME, M. B., LIND, C. H. & COLLINS, E. M. 2014. On-chip immobilization of planarians for in vivo imaging. *Scientific reports,* 4**,** 6388.

INOUE, T., YAMASHITA, T. & AGATA, K. 2014. Thermosensory signaling by TRPM is processed by brain serotonergic neurons to produce planarian thermotaxis. *J Neurosci,* 34**,** 15701-14.

KIM, I. V., ROSS, ERIC J., DIETRICH, SASCHA, DÖRING, KRISTINA, ALVARADO, ALEJANDRO SÁNCHEZ, KUHN, CLAUS-D. 2019. Efficient depletion of ribosomal RNA for RNA sequencing in planarians. *bioRxiv,* 670604.

LANGLOIS, V. S. & MARTYNIUK, C. J. 2013. Genome wide analysis of Silurana (Xenopus) tropicalis development reveals dynamic expression using network enrichment analysis. *Mechanisms of development,* 130**,** 304-22.

LANGMEAD, B. 2010. Aligning short sequencing reads with Bowtie. *Curr Protoc Bioinformatics,* Chapter 11**,** Unit 11 7.

LIU, S.-Y. & RINK, J. C. 2018. Total RNA Isolation from Planarian Tissues. *In:* RINK, J. C. (ed.) *Planarian Regeneration: Methods and Protocols.* New York, NY: Springer New York.

OVIEDO, N. J., NICOLAS, C. L., ADAMS, D. S. & LEVIN, M. 2008a. Establishing and maintaining a colony of planarians. *CSH Protoc.,* 2008**,** db.prot5053.

OVIEDO, N. J., NICOLAS, C. L., ADAMS, D. S. & LEVIN, M. 2008b. Live Imaging of Planarian Membrane Potential Using DiBAC4(3). *Cold Spring Harb Protoc,* 2008**,** pdb.prot5055-.

PAGAN, O. R., ROWLANDS, A. L. & URBAN, K. R. 2006. Toxicity and behavioral effects of dimethylsulfoxide in planaria. *Neurosci Lett,* 407**,** 274-8.

PFAFFL, M. W. 2001. A new mathematical model for relative quantification in real-time RT-PCR. *Nucleic Acids Res,* 29**,** e45.

STEVENS, A. S., PIROTTE, N., PLUSQUIN, M., WILLEMS, M., NEYENS, T., ARTOIS, T. & SMEETS, K. 2015. Toxicity profiles and solvent-toxicant interference in the planarian Schmidtea mediterranea after dimethylsulfoxide (DMSO) exposure. *J Appl Toxicol,* 35**,** 319-26.

TAKANO, T., PULVERS, J. N., INOUE, T., TARUI, H., SAKAMOTO, H., AGATA, K. & UMESONO, Y. 2007. Regeneration-dependent conditional gene knockdown (Readyknock) in planarian: demonstration of requirement for Djsnap-25 expression in the brain for negative phototactic behavior. *Dev Growth Differ,* 49**,** 383-94.

TRAPNELL, C., PACHTER, L. & SALZBERG, S. L. 2009. TopHat: discovering splice junctions with RNA-Seq. *Bioinformatics,* 25**,** 1105-11.

YUAN, Z., ZHAO, B. & ZHANG, Y. 2012. Effects of dimethylsulfoxide on behavior and antioxidant enzymes response of planarian Dugesia japonica. *Toxicol Ind Health,* 28**,** 449-57.